EBioMedicine 2 (2015) 406–420

Contents lists available at ScienceDirect

EBioMedicine

journal homepage: www.ebiomedicine.com

Original Article

MET Suppresses Epithelial VEGFR2 via Intracrine VEGF-induced Endoplasmic Reticulum-associated Degradation

Tom T. Chen [a], Ellen Filvaroff [a,1], Jing Peng [b], Scot Marsters [a], Adrian Jubb [c], Hartmut Koeppen [c], Mark Merchant [b], Avi Ashkenazi [a,*]

[a] Cancer Immunology, Genentech, Inc. 1 DNA Way, South San Francisco, CA 94080, USA
[b] In Vivo Pharmacology, Genentech, Inc. 1 DNA Way, South San Francisco, CA 94080, USA
[c] Research Pathology, Genentech, Inc. 1 DNA Way, South San Francisco, CA 94080, USA

ARTICLE INFO

Article history:
Received 7 March 2015
Received in revised form 26 March 2015
Accepted 27 March 2015
Available online 28 March 2015

Keywords:
HGF
VEGF
ERAD
PI3 kinase
AKT
MEK
IRE1
XBP1

ABSTRACT

Hepatocyte growth factor (HGF) and vascular endothelial growth factor (VEGF) drive cancer through their respective receptors, MET and VEGF receptor 2 (VEGFR2). VEGFR2 inhibits MET by promoting MET dephosphorylation. However, whether MET conversely regulates VEGFR2 remains unknown. Here we show that MET suppresses VEGFR2 protein by inducing its endoplasmic-reticulum-associated degradation (ERAD), via intracrine VEGF action. HGF–MET signaling in epithelial cancer cells promoted VEGF biosynthesis through PI3-kinase. In turn, VEGF and VEGFR2 associated within the ER, activating inositol-requiring enzyme 1α, and thereby facilitating ERAD-mediated depletion of VEGFR2. MET disruption upregulated VEGFR2, inducing compensatory tumor growth via VEGFR2 and MEK. However, concurrent disruption of MET and either VEGF or MEK circumvented this, enabling more profound tumor inhibition. Our findings uncover unique cross-regulation between MET and VEGFR2—two RTKs that play significant roles in tumor malignancy. Furthermore, these results suggest rational combinatorial strategies for targeting RTK signaling pathways more effectively, which has potentially important implications for cancer therapy.

1. Introduction

A number of growth factors and cognate receptor-tyrosine-kinases (RTKs) display genetic alterations in cancer and contribute to various aspects of tumor progression (Choura and Rebai, 2011; Takeuchi and Ito, 2011). Hepatocyte growth factor (HGF), also known as scatter factor, signals through the RTK MET, mainly to regulate epithelial-cell functions including motility, invasiveness, survival and proliferation (Gherardi et al., 2012). In contrast, vascular endothelial growth factor (VEGF), particularly VEGF-A, signals through the RTK VEGFR2, primarily to regulate endothelial cell activities that facilitate vasculogenesis, angiogenesis and vascular function (Carmeliet and Jain, 2011; Ellis and Hicklin, 2008; Ferrara et al., 2003). Aberrant MET stimulation in tumor epithelial cells, via activating mutations, gene amplification and/or mRNA and protein overexpression, increases tumor aggressiveness and correlates with poor prognosis (Gherardi et al., 2012; Sadiq and Salgia, 2013). On the other hand, VEGF production by malignant epithelial cells or associated stromal cells enables the formation and maintenance of vascular networks that support tumor growth. Although VEGFR2 is expressed most frequently on tumor endothelial cells (Smith et al., 2010), it can be expressed also by malignant epithelial cells, and promotes their proliferation—for example, in concert with signaling by epidermal growth factor receptor (EGFR) (Goel and Mercurio, 2013; Lichtenberger et al., 2010). Germline variations in the VEGFR2 gene alter expression of VEGFR2 protein in tumor endothelial and epithelial cells, as well as VEGFR2's involvement in tumor vascularization (Glubb et al., 2011).

Beyond individual RTK contributions, evidence suggests that crosstalk between different RTKs augments tumor growth and promotes resistance to conventional or targeted therapies (Chong and Janne, 2013; Engelman et al., 2007; Wilson et al., 2012). MET interacts functionally with several RTKs, including EGFR, ERBB2 and IGF-1R (Bauer et al., 2006; Boon et al., 2002; Engelman et al., 2007; Khoury et al., 2005; Liu et al., 2009; Yamamoto et al., 2006). EGFR stimulation drives MET phosphorylation (Yamamoto et al., 2006), while MET-gene amplification in lung cancer cells harboring resistance-conferring EGFR mutations activates ERBB3–PI3-kinase (PI3K) signaling (Engelman et al., 2007). Combined EGFR and MET inhibition showed enhanced efficacy against human NSCLC tumor xenografts in mice (Turke et al., 2010). In a phase II clinical study, concurrent treatment with the EGFR inhibitor erlotinib and the anti-MET antibody onartuzumab improved survival as compared to erlotinib monotherapy in a subset of NSCLC patients expressing high tumor

* Corresponding author.
E-mail address: aa@gene.com (A. Ashkenazi).
[1] Current address: Celgene, San Francisco, CA, USA.

http://dx.doi.org/10.1016/j.ebiom.2015.03.021

levels of MET (Spigel et al., 2013); however, a subsequent phase III trial did not recapitulate this latter finding (ASCO 2014). VEGFR2 and MET also can cross-interact: in glioblastoma multiforme cells, VEGFR2 inhibits MET phosphorylation through enhanced recruitment of protein tyrosine phosphatase 1B, thereby suppressing MET-dependent tumor invasiveness (Lu et al., 2012). It remains unknown, however, whether MET reciprocally regulates VEGFR2—and if so—then how and to what consequence. We demonstrate here that MET suppresses VEGFR2 in epithelial cancer cells expressing both RTKs, through a unique, cell-autonomous mechanism involving intracrine VEGF and endoplasmic reticulum associated degradation or ERAD. MET disruption upregulates VEGFR2, which drives compensatory tumor growth. Importantly, this undesired outcome of MET disruption can be blocked by concurrent inhibition of the MET and VEGFR2 pathways. Our results underscore the potential of combinatorial RTK inhibition to enhance anti-tumor efficacy. More specifically, our data provide translational strategies for increasing the efficacy of therapeutic modalities targeting the HGF–MET and VEGF–VEGFR2 pathways in cancer.

2. Materials and Methods

2.1. Patient Tumor Samples

Formalin-fixed paraffin-embedded tissues from 31 non-small cell lung cancers (9 adenocarcinomas, 3 adenosquamous carcinomas, 13 squamous cell carcinomas and 6 large cell carcinomas) were obtained from multiple sources (Advanced Bioscience Laboratories, Kensington, MD; University of Michigan, Ann Arbor, MI; Cureline, South San Francisco, CA; Cooperative Human Tissue Network, Nashville, TN; ProteoGenex, Culver City, CA; Cytomix (Origene), Rockville, MD; MT Group, Van Nuys, CA, USA). Histological diagnosis was confirmed centrally by a pathologist (H.K.).

2.2. Cell lines and Cell Culture

H441, C829, C32, PC-3, H1838 and H2347 were purchased from ATCC. PSN1, UM-UC-1 and UM-UC-3 cells were purchased from ECACC. RERF_LC, EBC1 and KP4 were purchased from JHSF. The NSCLC cell line LKPH4 was derived from a $KRas^{LSL\text{-}G12D/+}$;$p53^{FL/+}$;Z/EG lung tumor-bearing mouse. H441 cells were cultured in F12/DMEM (50:50) with 10% Fetal Bovine Serum and 2 mM L-glutamine. C829, C32, PC-3, H1838, H2347, PSN1, UM-UCs, RERF_LC, EBC1 and KP4 were cultured in RPMI 1640 with 10% Fetal Bovine Serum and 2 mM L-glutamine. LKPH4 cells were cultured in DMEM high glucose with 10% FBS and 2 mM L-glutamine. Cells grown under hypoxia were incubated for 48 h under an atmosphere of 5% CO_2-balanced N_2 to obtain 1% O_2 at 37 °C. Otherwise grown under normoxia at 37 °C, 5% CO_2.

2.3. Reagents

Recombinant human $VEGF_{165}$ and HGF were generated and purified at Genentech (South San Francisco, CA). Antibodies against human VEGFR2, phospho-VEGFR2 (Tyr1175), MET, phospho-MET (Tyr1234/1235), Akt, phospho-Akt (S473), Rab5/8/9, Cbl, Cbl-b, ubiquitin, Gab1, phospho-Gab1, PLC, phospho-PLC, MEK, phospho-MEK, ERK, phospho-ERK, phospho-S6, EGFR, PERK, CHOP and BIP were from Cell Signaling (Beverly, MA). Anti-ATF6 was from Cosmo Bio Co. (Tokyo, Japan). Antibodies against phosphotyrosine (4G10) and GAPDH were from Millipore (Billerica, MA). Antibodies against actin, tubulin, and VEGFR1 were from Abcam (Cambridge, MA). Mouse anti-VEGF was from Origene (Rockville, MD). Rabbit anti-VEGFR2 (N-terminus) was from Cell Sciences (Canton, MA). FGFR1 antibody was from Santa Cruz Biotechnology (Santa Cruz, CA). Antibodies against ER marker (P4HB/PDI), Golgi marker (GOLGA2), gp78 (AMFR), and HRD1 (SYVN-1) were purchased from Sigma Aldrich (St. Louis, MO). K48-ubiquitin, XBP-1s, phosphor-IRE1 α antibodies were generated and purified at Genentech. MG132 and Dynasore were from Calbiochem (La Jolla, CA). Small molecule inhibitors (SMI) against MET (GDC0712), PI3K (GDC0941), MEK (cobimetinib), JAK (G00043484), and IRE1α (compound 3 and 4μ8c) were synthesized for Genentech. SU4312 was from Enzo (Farmingdale, NY). Leupeptin and pepstatin A were from Sigma Aldrich. E-64d was from Cayman Chemicals (Ann Arbor, Michigan).

2.4. Mouse Studies

Five million H441.shMet 3.11 cells suspended in HBSS were inoculated subcutaneously in the right flank of CRL nu/nu mice (Charles River Laboratories). When tumors reached an average volume of ~250 mm^3, mice (8 per group) were treated with either 5% sucrose water (provided as drinking water, changed weekly) plus MCT ((0.5% [w/v] methylcellulose, 0.2% [w/v] polysorbate 80 [Tween-80], 0.1 ml, daily, oral gavage), Doxycycline (0.2 mg/ml, dissolved in 5% sucrose water, changed 3×/week), B20-4.1.1 (anti-VEGF antibody, 5 mg/kg, intraperitoneal, 2×/week), or cobimetinib (MEKi, 5 mg/kg, daily orally dosed for the duration of the study), or the combination of Doxycycline plus B20-4.1.1 or Doxycycline plus cobimetinib. Tumor volumes were measured in two dimensions (length and width) using Ultra Cal IV calipers (Model 54 10 111; Fred V. Fowler Company; Newton, MA). The tumor volume was calculated using the following formula: tumor volume (mm^3) = (length × $width^2$) × 0.5. All procedures were approved by and conformed to the guidelines and principles set by the Institutional Animal Care and Use Committee of Genentech and were carried out in an Association for the Assessment and Accreditation of Laboratory Animal Care (AAALAC)-accredited facility.

2.5. Generation of Cell Lines Stably Expression Dox-inducible MET shRNA

Two independent MET shRNA were cloned into pHUSH vector as described (Pai et al., 2008). The sequence used in the studies is as follows.

shMET 3	5′-GATCCCC**GAACAGAATCACTGACATA**TTCAAGAGA**TATGTC AGTGATTCTGTTC**TTTTTTGGAAA-3′
shMET 4	5′-GATCCCC**GAAACTGTATGCTGGATGA**TTCAAGAGA**TCATCC AGCATACAGTTTC**TTTTTTGGAAA-3′
shGFP2 EGFP shRNA (sense)	5′-GATCCCCAGATCCGCCACAACATCGATTCAAGAGATCGAT GTTGTGGCGGATCTTGTTTTTTGGAAA-3′

All constructs were confirmed by sequencing. EGFP control shRNA was described previously (Pai et al., 2008). The shRNA containing retrovirus was produced by co-transfecting GP2-293 packaging cells (Clontech Laboratories, Mountain View, CA) with VSV-G (Clontech Laboratories) and pHUSH-MET shRNA constructs. Viral supernatants were harvested 72 h after transfection, and cleared of cell debris by centrifugation for transduction.

H441 cells were maintained in F12/DMEM 50/50 medium containing tetracycline-free FBS (Clontech Laboratories), and transduced with retroviral supernatant in the presence of 4 μg/ml polybrene. 72 h after infection, 2 μg/ml puromycin (Clontech Laboratories) was added to the medium to select stable clones expressing shRNA. Clones were isolated, treated with 0.1 or 1 μg/ml doxycycline (Clontech Laboratories) for 4 days, and inducible knockdown of MET protein was assessed by immunoblot analysis. Cell cycle analyses were performed as described (Pegram et al., 1999).

2.6. Patient-derived Tumor Xenograft Microarray Analysis

Patient-derived lung tumor xenograft samples were analyzed using Affymetrix Human Genome U133 Plus 2.0 arrays. The Bioconductor

package affy (Gautier et al., 2004) was used for obtaining RMA-normalized expression data. For both MET and VEGFR2 a uniquely mapped probe set was used.

2.7. Immunoblotting and Immunoprecipitation

Cells were lysed in RIPA buffer (50 mM Tris, pH 7.4, 150 mM NaCl, 1% NP-40, 0.25% sodium deoxycolate, 1 mM EDTA, 1 mM sodium vanadate, 10 mM ß-glycerophosphate, and protease inhibitors (Thermo Fisher Scientific, Pittsburgh PA). To deglycosylate the denatured protein, the sample was treated using either Endoglycosidase H (Endo H) or peptide *N*-glycosidase F (PNGaseF; New England Biolabs, Ipswich, MA) according to the manufacturer recommendations. Both deglycosylated and untreated samples were subjected to SDS-PAGE. For immunoprecipitation, cell lysates were further incubated under agitation at 4 °C for 30 min, and then centrifuged at 20,000 *g* for 30 min at 4 °C. Equivalent levels (500 μg) of protein, determined using the DC protein assay reagent (Bio-Rad Labs, Hercules, CA), were precleared by anti-Rabbit Ig IP Dynabeads (Life technologies, Grand Island, NY) and immunoprecipitated overnight at 4 °C with indicated antibody. Immune complexes were retrieved using anti-Rabbit Ig IP Dynabeads. Immunoprecipitates were washed three times with same lysis buffer and then separated by SDS-PAGE. Proteins were transferred to nylon membranes (Bio-Rad), probed with indicated antibodies, and detected using a ChemiDoc™ MP Imaging System and enhanced chemiluminescence (Bio-Rad). After detection, the results were quantified by densitometry using ImageJ (NIH, Bethesda, Maryland).

Protein phosphorylation was usually determined by immunoblotting as described previously (Luque et al., 2003). VEGFR2 autophosphorylation was analyzed in presence of 100 μM activated sodium ortho-vanadate (Gordon, 1991) for 24 h at 37 °C. Phospho-VEGFR2 was then analyzed by IP with anti-VEGFR2 followed by immunoblot with anti-phosphotyrosine antibody, or by sandwich ELISA using the human phospho-VEGFR2/VEGFR2 Duoset IC kit (R&D). Antibody detection of K48-linked ubiquitin was performed by IP with anti-K48-ubiquitin antibody as described previously (Gonzalvez et al., 2012).

2.8. Transfection With siRNA Oligonucleotides

The siRNA oligonucleotides against human VEGFA, VEGFR2, MET, Cbl, Cbl-b, gp78, HRD1, were from Dharmacon (Lafayette, CO):

Non-targeting control (NTC)1: 5′ CTT ACG CTG AGT ACT TCG A-dTdT 3′

siVEGFA Smartpool: L-003550
siVEGFR2 #1: J-003148-09
siVEGFR2 #2: J-003148-10
siVEGFR2 #3: J-003148-11
siVEGFR2 #4: J-003148-12
siMET Smartpool: L-003156
siCbl Smartpool: L-003003
siCbl-b Smartpool: L-003004
sigp78 Smartpool: L-006522
siHRD1 Smartpool: L-007090
sip97/VCP Smartpool: L-008727.

Cells were transfected using Transfectant #2 (Dharmacon) according to the manufacturer's protocol.

2.9. Proximity Ligation Assay (PLA)

H441 cells grown on Lab-TekII chamberslides (Thermo Fisher Scientific) were incubated in the presence or absence of HGF (100 ng/ml) overnight at 37 °C in serum-free media. Cells were fixed with 4% paraformaldehyde for 15 min, with or without permeabilization, blocked, incubated overnight with mouse anti-VEGF (Origene) and rabbit anti-VEGFR2 (Cell Sciences). Proximity ligation was performed using the Duolink Detection Kit with PLA PLUS and MINUS Probes for mouse and rabbit (Olink Bioscience, Uppsala, Sweden) according to the manufacturer's protocol. Slides were mounted with Prolong Gold antifade reagent with DAPI and examined with a Zeiss AxioImager M2 fluorescence microscope under a 63× oil objective, using Slidebook software to acquire images. Images were then analyzed and red dots counted by NIH ImageJ. Eight fields at 600× were randomly chosen for analysis and averaged per condition examining four independent preparations individually.

To counterstain with ER, Golgi, or Rab antibodies, PLA was performed as previously described without mounting; samples were then incubated with primary anti-ER, anti-Golgi or indicated anti-Rab antibodies (1:100) at room temperature for 2 h, washed 2 times with PLA wash buffer A and incubated with fluorophore-linked secondary antibodies at room temperature for 1 h. Samples were washed again 2 times with PLA buffer A and once with PLA buffer B. Slides were then mounted with Prolong Gold anti-fade reagent containing DAPI and viewed with a LEICA SP5 inverted confocal microscope under a 63× oil objective, using Leica LAS AF software to acquire images.

2.10. Immunocytochemistry and Confocal Microscopy

H441 cells were grown on Lab-TekII chamberslides (Thermo Fisher Scientific) and treated as indicated. Cultures were fixed with 4% paraformaldehyde for 15 min at room temperature and permeabilized with 0.2% saponin in blocking buffer (10% goat serum, 10 mM Hepes, 10 mM glycine in RPMI 1640) for 15 min at room temperature. Slides were then washed and blocked in blocking buffer for 1 h at room temperature. Indicated antibodies were diluted in blocking buffer incubated with cells at 4 °C overnight. After three washes with PBS, cells were incubated with respective 1:100 diluted secondary antibodies conjugated with either Alexa488 or Alexa647 (Invitrogen). F-actin was detected using Alexa 555 conjugated phalloidin (Invitrogen) diluted 1:40 in blocking buffer. Slides were mounted with Prolong Gold anti-fade reagent containing DAPI and viewed with a LEICA SP5 inverted confocal microscope under a 63× oil objective, using Leica LAS AF software to acquire images.

2.11. Quantitation of Co-localized Signal

Images were collected randomly (10 images from each treatment; 3 independent experiments), and colocalization was determined with the "Colocalization" Plug-in of ImageJ (NIH) with the same color-threshold settings for all 10 images from each treatment. The co-localized color channel (blue) and PLA color channel (green) or both red and green channels (for ICC) were then counted with the "Analyze particles" command of Image J. Percent colocalization was then calculated by total area of co-localized channel (blue) over total area of PLA channel (green) or both red and green channels (for ICC).

2.12. VEGF ELISA

To quantify levels of VEGF in the conditioned medium and cell layers, cells were cultured in complete medium containing 10% FBS at 37 °C until subconfluent. Medium containing 0.1% FBS was then added and collected after 24 h of incubation at 37 °C. The conditioned medium was removed and centrifuged at 4 °C for 60 min at 13,200 rpm. The supernatant was then collected and assayed by using a sandwich human VEGF-ELISA kit (R&D). Cell lysates were collected as above and assayed by the same kit.

2.13. Cell Proliferation Assay

H441 cells were cultured on a 96-well plate and imaged using a real-time imaging system (IncuCyte™, Essen Bioscience, Ann Arbor, Michigan). Frames were captured at 4-h intervals from 2 separate 950 × 760-μm^2 regions per well using a 10× objective. Cultures were maintained at 37 °C throughout and run in sextuplicate. H441 cells confluence was then measured before and after the treatment. Values from both regions of each well were pooled and averaged across all 6 replicates.

2.14. Statistical Methods

Data and graph were evaluated using a student's two-tailed t-test or ANOVA with GraphPad Prism 6 software (San Diego, CA). In all analyses, $p < 0.05$ was taken to be statistically significant.

2.15. Funding

All work was funded by Genentech, Inc.

3. Results

3.1. MET Activity Suppresses VEGFR2

Elevated MET expression is detected in diverse cancer types, including ~60% of non-small cell lung carcinomas (NSCLC) (Gherardi et al., 2012; Sadiq and Salgia, 2013). We verified MET expression by immunohistochemistry (IHC) in both epithelial and endothelial compartments of NSCLC tumor tissues (Figs. 1A and S1A). To examine VEGFR2 expression more closely, we first analyzed 31 primary NSCLC tumor samples by VEGFR2 IHC and in-situ hybridization (ISH). While most of the tumors displayed endothelial VEGFR2 expression (data not shown), we

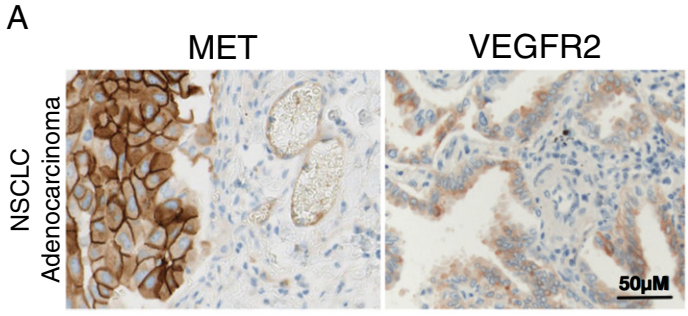

B

NSCLC subtypes	# of Samples	Samples with epithelial VEGFR2	% epithelial VEGFR2
Adenocarcinoma	9	3	33.3%
Adenosquamous	3	0	0%
Squamous Carcinomas	13	0	0%
Large cell carcinoma	6	0	0%
Total	31	3	9.7%

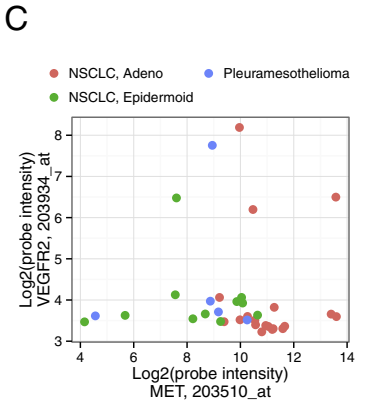

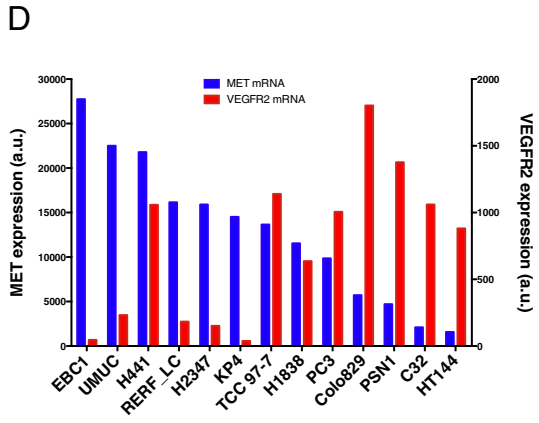

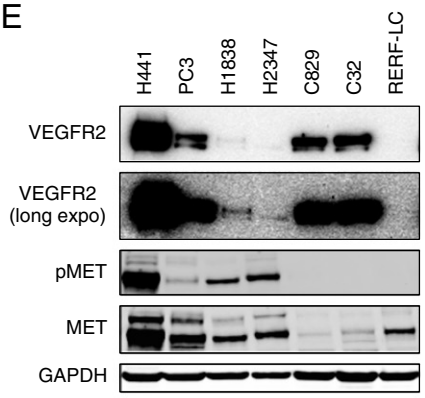

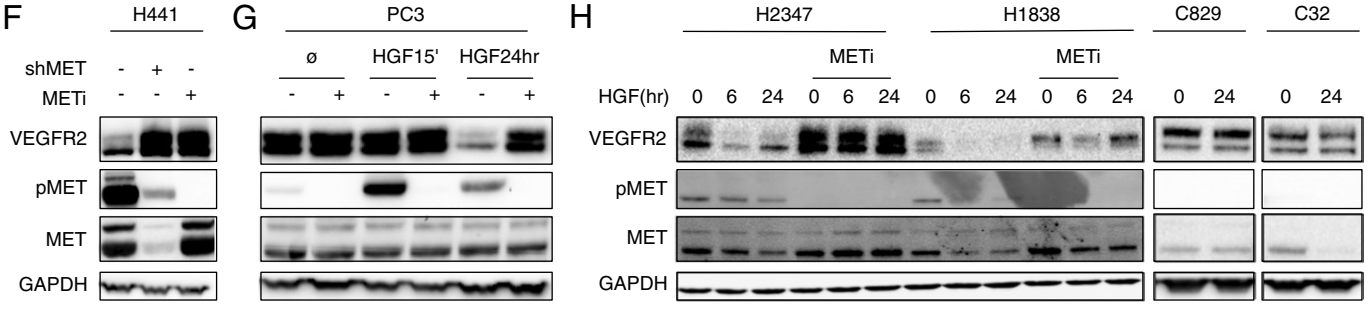

Fig. 1. Expression of MET and VEGFR2 in epithelial cancer cells and suppression of VEGFR2 by HGF–MET signaling. (A) Immunohistochemical (IHC) analysis of MET and VEGFR2 expression in an example of primary NSCLC adenocarcinoma. (B) Summary of VEGFR2 expression as determined by IHC in NSCLC patient tumor samples. (C) Expression of MET and VEGFR2 mRNAs in patient-derived lung tumor samples xenografted in mice. (D) Expression levels of MET (blue) and VEGFR2 (red) mRNA (a.u., arbitrary units) in cancer cell lines based on microarray analysis data. (E) Immunoblot analysis of VEGFR2, MET and phospho-MET (pMET) in cell lines that display high mRNA levels of MET and VEGFR2. (F) H441 cells were treated with Dox to induce shRNA-based MET knockdown (shMET) or with 1 μM MET SMI (GDC-0712) for 48 h and analyzed by immunoblot. (G) Cells were treated with HGF (100 ng/ml) for 15 min or 24 h in the absence (all) or presence (PC3) of METi (GDC-0712, 1 μM) and levels of VEGFR2, pMET and MET were analyzed by immunoblot. (H) Cells were treated as in F and amounts of VEGFR2, pMET and MET were analyzed by immunoblot.

detected significant epithelial VEGFR2 protein and mRNA expression in 33.3% of adenocarcinomas, though not in squamous cell carcinomas (Figs. 1B and S1B). We also analyzed mRNA from additional patient-derived tumors xenografted in mice: 3 of 19 (15.8%) lung adenocarcinomas; 1 of 11 (9.1%) lung epidermoid carcinomas; and 1 of 5 (20%) pleuromesotheliomas showed elevated expression of MET and VEGFR2 mRNA (Fig. 1C). To identify suitable models for investigating potential cross-regulation between MET and VEGFR2, we first examined a panel of epithelial cancer cell lines for mRNA expression of both RTKs based on microarray analysis (Fig. 1D). We then tested some of these cell lines for protein expression by immunoblot (Fig. 1E). H441 and PC3 cells strongly expressed both VEGFR2 and MET, while H1838 and H2347 expressed lower yet detectable amounts of both proteins. By contrast, C829 and C32 cells strongly expressed VEGFR2 without detectable MET, whereas RERF-LC cells expressed no detectable VEGFR2 and low levels of MET. ISH and IHC analyses confirmed significant VEGFR2 expression in H441 cells, albeit at lower abundance than in human umbilical vein endothelial cells (HUVEC), with no detectable expression in HT29 cells (Fig. S1C). Thus, a notable subset of patient-derived tumors and cancer cell lines exhibits epithelial co-expression of MET and VEGFR2.

To begin to investigate whether MET regulates VEGFR2, we generated H441 cell lines harboring a stable, doxycycline (Dox)-inducible MET shRNA (H441 shMET) (Fig. S1D,E). Untreated H441 cells exhibited constitutive MET phosphorylation, which was inhibited by Dox-induced MET knockdown or addition of a small molecule inhibitor (SMI) of MET kinase, GDC0712 (Liederer et al., 2011) (Fig. 1F). Strikingly, MET knockdown or inhibition substantially increased VEGFR2 protein levels, without affecting several other RTKs, i.e. VEGFR1, FGFR1 and EGFR (Figs. 1F and S1D–F). Unlike H441 cells, PC3 cells did not exhibit significant constitutive MET phosphorylation; however, HGF treatment of PC3 cells induced MET phosphorylation within 15 min, subsiding by 24 h (Fig. 1G). Conversely to the upregulation of VEGFR2 upon MET disruption, MET stimulation by HGF caused dramatic depletion of VEGFR2 protein by 24 h (Fig. 1G). Similarly, HGF treatment downregulated VEGFR2 within 6–24 h in H2347 and H1838 cells, and this suppression was reversed by MET inhibition (Fig. 1H). In contrast, HGF had minimal impact on VEGFR2 levels in C829 and C32 cells, which expressed readily detectable VEGFR2 but little MET (Fig. 1H). Nevertheless, transfection of C32 cells with cDNA constructs directing expression of full-length MET led to dose-dependent suppression of VEGFR2 (Fig. S1G). Thus, constitutive or HGF-induced MET activity suppresses VEGFR2 protein levels in epithelial tumor cell lines that express both RTKs.

3.2. MET Suppresses VEGFR2 via Intracrine VEGF Action

Previous work indicates that HGF can promote VEGF expression (Zhang et al., 2003). We therefore examined the possibility that MET might control VEGFR2 levels via VEGF activity. Untreated H441 cells secreted significant amounts of VEGF protein into the conditioned culture media (Fig. 2A). MET inhibitor markedly attenuated VEGF secretion, whereas HGF treatment increased VEGF amounts by ~2 fold, in a manner that was attenuated by MET inhibition. PC3 cells produced low baseline amounts of VEGF, which were unaffected by MET inhibition; however, HGF treatment upregulated VEGF secretion by ~2.5 fold, and this increase was attenuated by MET inhibition (Fig. 2A). Further analysis of H441 cells revealed that perturbation of MET, but not VEGFR2, led to a marked drop in both secreted and cellular VEGF protein pools (Figs. 2B, S2A and S2B). MET disruption also decreased VEGF mRNA (Fig. 2C). Thus, MET promotes de novo transcription, biosynthesis and secretion of VEGF.

We next sought to interrogate whether the induction of VEGF production and the suppression of VEGFR2 by MET were mechanistically linked. Several intracellular RTK signaling cascades, including the PI3K/AKT, MEK/ERK and JAK/STAT pathways, may regulate VEGF production in response to specific growth factors (Dong et al., 2001; Eder et al., 2009; He et al., 2006; Jiang et al., 2000; Kowanetz and Ferrara, 2006; Zhang et al., 2010). SMI disruption of PI3K, but not MEK or JAK, substantially attenuated HGF-induced VEGF production in PC3 cells (Figs. 2D and S2C). Remarkably, PI3K SMI, but not MEK or JAK SMIs, efficiently blocked VEGFR2 suppression in response to HGF (Fig. 2E). Similarly, MET or PI3K SMI exerted dose-dependent attenuation of MET-driven VEGF production—and coincidently, VEGFR2 suppression—in H441 cells (Figs. 2F,G and S2D). Thus, MET signaling upregulates VEGF biosynthesis via the PI3K pathway—an event that correlates with VEGFR2 depletion. However, a direct causal link between VEGF induction and VEGFR2 suppression remained to be investigated.

To test whether VEGF induction could downregulate VEGFR2, we used two gain-of-function strategies. First, ectopic VEGF expression by cDNA transfection of H441 cells substantially reversed the upregulation of VEGFR2 upon MET perturbation (Fig. 2H). Second, oxygen deprivation, which drives VEGF production via hypoxia-inducible factor (HIF)-1α (Forsythe et al., 1996), prevented the drop in VEGF secretion caused by MET knockdown in H441 cells (Fig. 2I). Moreover, hypoxia blocked upregulation of VEGFR2 upon MET disruption, and this effect was reversed by siRNA knockdown of VEGF (Fig. 2J). Hence, either ectopic VEGF expression, or—more physiologically—hypoxia-induced production of endogenous VEGF, suppresses VEGFR2 protein, supporting a possible mechanistic role for VEGF.

To address causal involvement of VEGF more directly, we asked whether its depletion by different methods affects MET-driven suppression of VEGFR2. Surprisingly, addition of an anti-VEGF antibody, which neutralized essentially all the detectable extracellular VEGF (Fig. S2E), had little impact on VEGFR2 upregulation in response to MET disruption in H441 cells (Fig. 2K). In contrast, siRNA knockdown of VEGF increased baseline VEGFR2 levels, but did not further augment VEGFR2 upregulation upon MET disruption (Figs. 2K and S2E). These results indicate that MET and VEGF operate along the same axis and that MET-induced VEGF plays a critical role in VEGFR2 suppression. Furthermore, intracellular (i.e., intracrine), rather than extracellular (i.e. autocrine or paracrine) VEGF activity mediates the depletion of VEGFR2. Consistent with this latter notion, addition of exogenous VEGF to H441 or PC3 cells failed to alter basal VEGFR2 levels or modulation by MET (Fig. S2F,G), in contrast to the marked VEGFR2 downregulation induced by transfected or hypoxia-induced VEGF (Fig. 2H and J).

Endocytosis plays a key role in VEGFR2 activation by extracellular VEGF (Chen et al., 2010; Sawamiphak et al., 2010). MET knockdown or inhibition modestly upregulated cell-surface levels of VEGFR2, as indicated by FACS and subcellular fractionation analyses (Fig. S2H,F). However, disruption of clathrin-mediated endocytosis with the

Fig. 2. MET suppresses VEGFR2 via PI3K-induced intracrine VEGF action. (A) Effect of HGF (100 ng/ml), METi (GDC-0712, 1 μM) or combinations thereof on VEGF secretion by PC3 and H441 cells after 24 h treatment. (B) Effect of MET or VEGFR2 knockdown on VEGF production. H441 cells were subjected to knockdown of MET (shMET) or VEGFR2 (siVEGFR2) or both for 2 days and VEGF protein levels in conditioned media or washed cell monolayers were measured by ELISA. (C) Effect of MET disruption on mRNA levels of MET and VEGF. H441 cells were subjected to MET inhibition (METi) or knockdown (shMET) and mRNA levels were determined by qPCR. (D and E) Effect of 1 μM of MET, PI3K, MEK, or JAK SMI on modulation of VEGF (D) and VEGFR2 (E) by HGF. PC3 cells were treated with PBS or HGF (100 ng/ml) for 24 h and VEGF levels in washed cell layers were determined as above (D), while levels of VEGFR2 or other indicated markers were determined by immunoblot (E). (F and G) Effect of MET SMI (F) or PI3K SMI (G) on secreted levels of VEGF (bar graphs) or VEGFR2 (immunoblots) in H441 cells. 1× is 1 μM for METi and 10 μM for PI3Ki. (H) Effect of VEGF transfection on VEGFR2 modulation by MET shRNA knockdown (shMET) or kinase inhibition (METi, 1 μM) in H441 cells. (I) Effect of MET knockdown (shMET) in H441 cells cultured under normoxia or hypoxia on VEGF levels in washed cell layers. (J) Effect of MET knockdown (shMET) or inhibition (METi, 1 μM) on VEGFR2 levels in H441 cells cultured under normoxia or hypoxia with or without siRNA knockdown of VEGF. (K) Effect of extracellular VEGF neutralization (anti-VEGF, 10 μg/ml) or VEGF siRNA knockdown (siVEGF) on VEGFR2 modulation by MET knockdown (shMET) or inhibition (METi, 1 μM) in H441 cells. Scrambled siRNA (siNTC) was used as control. Error bars indicate S.E.M for a minimum of three independent experiments. *$p < 0.05$, **$p < 0.01$, and ***$p < 0.005$ for indicated comparisons.

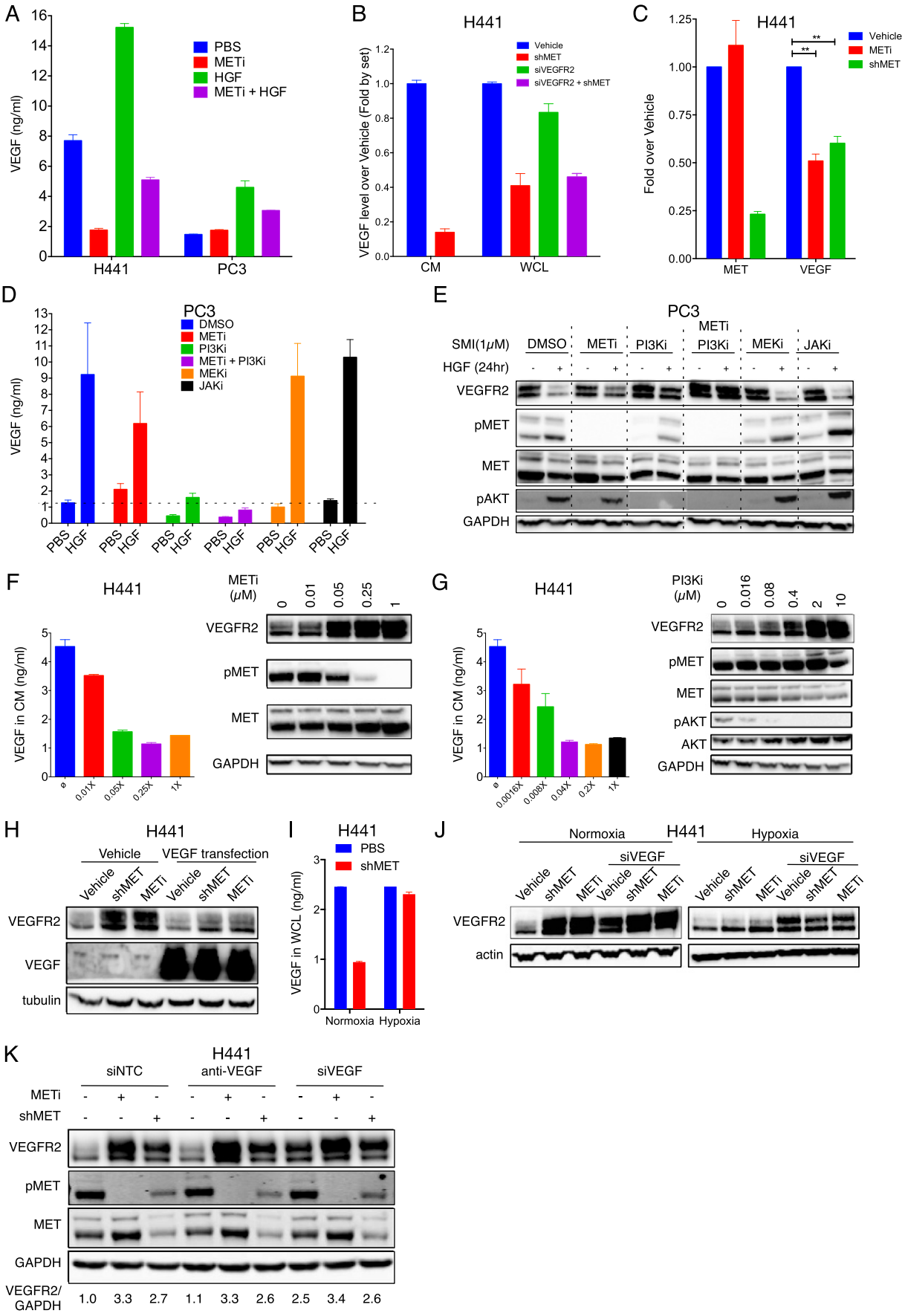
A
VEGF (ng/ml)
PBS
METi
HGF
METi + HGF
H441
PC3
B
H441
VEGF level over Vehicle (Fold by set)
Vehicle
shMET
siVEGFR2
siVEGFR2 + shMET
CM
WCL
C
H441
Fold over Vehicle
Vehicle
METi
shMET
MET
VEGF
D
PC3
VEGF (ng/ml)
DMSO
METi
PI3Ki
METi + PI3Ki
MEKi
JAKi
PBS
HGF
E
PC3
METi
SMI(1μM)
DMSO
METi
PI3Ki
PI3Ki
MEKi
JAKi
HGF (24hr)
VEGFR2
pMET
MET
pAKT
GAPDH
F
H441
METi (μM)
0
0.01
0.05
0.25
1
VEGF in CM (ng/ml)
VEGFR2
pMET
MET
GAPDH
G
H441
PI3Ki (μM)
0
0.016
0.08
0.4
2
10
VEGF in CM (ng/ml)
VEGFR2
pMET
MET
pAKT
AKT
GAPDH
H
H441
Vehicle
VEGF transfection
Vehicle
shMET
METi
VEGFR2
VEGF
tubulin
I
H441
PBS
shMET
VEGF in WCL (ng/ml)
Normoxia
Hypoxia
J
H441
Normoxia
Hypoxia
siVEGF
Vehicle
shMET
METi
VEGFR2
actin
K
H441
siNTC
anti-VEGF
siVEGF
METi
shMET
VEGFR2
pMET
MET
GAPDH
VEGFR2/ GAPDH
1.0 3.3 2.7 1.1 3.3 2.6 2.5 3.4 2.6

dynamin inhibitor dynasore did not affect VEGFR2 modulation by MET (Fig. S2I), supporting the independence of this function from extracellular VEGF. Together, these results indicate that MET suppresses VEGFR2 via intracellular action of VEGF.

3.3. MET Induces Intracellular Interaction of VEGF and VEGFR2

The implication of intracellular VEGF in VEGFR2 depletion suggested that the two proteins might interact within HGF-stimulated and/or MET-active cells. To address this possibility, we first validated suitable antibodies for detection of intracellular VEGF and VEGFR2 under various conditions (Fig. S3A–C). Next, we used these antibodies to determine the relative cellular distribution of the two proteins by immunofluorescence. Upon HGF treatment of PC3 cells, VEGF and VEGFR2 displayed significant intracellular co-localization (Fig. 3A). VEGF also showed marked co-localization with the specific ER marker P4HB/PDI, but not the Golgi marker GOLGA2 (Fig. 3B). To investigate whether VEGF and VEGFR2 directly interact with each other, we used a DNA-oligonucleotide-based proximity-ligation assay (PLA), in which detection of two proteins generates an immunofluorescence signal only if they are within a few nanometers of each other (Soderberg et al., 2006). PLA analysis of PC3 cells showed that HGF treatment induced an intracellular interaction between VEGF and VEGFR2 (Fig. 3C); the PLA signal increased in permeabilized, but not non-permeabilized, cells, indicating that the two proteins associated with each other within the cells. HGF-induced VEGF:VEGFR2 complexes coincided with P4HB, but not GOLGA2 (Fig. 3D). Importantly, the intracellular co-localization of VEGF and VEGFR2 was unabated by addition of anti-VEGF antibody (Fig. S3D), demonstrating that this interaction was independent from extracellular VEGF. PLA counterstaining with antibodies against certain Rab proteins to mark specific intracellular vesicular compartments revealed HGF-driven VEGF:VEGFR2 association in conjunction with Rab8, but not Rab5 or Rab9 (Figs. 3E, S3E,F). Thus, HGF induces interaction between VEGF and VEGFR2 at the ER, perhaps during or after parallel folding or maturation of the two newly synthesized proteins. Additional interaction is detected in Rab8-positive secretory vesicles, suggesting some anterograde transport of the complex from the ER toward the Golgi compartment.

3.4. MET Drives Phosphorylation, K48 Ubiquitination and Degradation of VEGFR2

We next investigated whether the intracellular VEGF–VEGFR2 association in response to HGF might lead to post-translational modifications of VEGFR2. Unlike VEGF, which promoted significant VEGFR2 phosphorylation in H441 cells within 10–15 min of exposure, HGF did not drive rapid VEGFR2 phosphorylation (data not shown). However, a 24-h exposure to either VEGF or HGF induced a significant increase in VEGFR2 phosphorylation, as detected by anti-phospho-tyrosine IB analysis of VEGFR2 IP (Fig. 4A), or a more sensitive sandwiched-ELISA technique (see Supplemental Experimental Procedures) (Fig. 4B and C). Addition of anti-VEGF antibody, which blocked VEGFR2 phosphorylation in response to exogenous VEGF, did not significantly inhibit VEGFR2 phosphorylation in response to HGF in H441 or PC3 cells (Fig. 4B and C). In contrast, siRNA knockdown of VEGF attenuated HGF-induced VEGFR2 phosphorylation (Fig. 4B and C). These results suggest that intracrine VEGF activity induced by HGF drives phosphorylation of VEGFR2.

Biosynthesis of transmembrane proteins such as VEGFR2 typically involves partial N-linked glycosylation in the ER, followed by further modification and elaboration of the N-linked sugars in the Golgi compartment. To examine which pool of VEGFR2 is subjected to MET-driven suppression, we treated cell lysates with Endoglycosidase H (Endo H), which cleaves only immature N-glycans, or Peptide-*N*-Glycosidase F (PNGaseF), which cleaves all N-glycans. Undigested VEGFR2 migrated as two major protein bands—representing partially and fully glycosylated VEGFR2—both of which were enriched upon MET disruption (Fig. 4D). Endo H treatment completely depleted the partially glycosylated VEGFR2 band, giving rise to a lower-MW band representing deglycosylated VEGFR2 (Fig. 4D); in contrast, PNGaseF treatment collapsed both bands into the deglycosylated form of VEGFR2. These results suggest that MET suppression operates at the level of the ER-associated pool of partially glycosylated VEGFR2 polypeptides.

At the cell surface, VEGF-induced phosphorylation of VEGFR2 leads to receptor internalization, ubiquitination and proteasomal degradation (Duval et al., 2003), or alternatively, recycling to the plasma membrane through a VE-cadherin linked pathway (Gavard and Gutkind, 2006). We reasoned that the suppression of VEGFR2 by MET also might entail proteasomal degradation—a process frequently involved in RTK modulation (Bonifacino and Weissman, 1998). Indeed, the proteasome inhibitor MG132, but not a lysosome-inhibitor cocktail containing leupeptin, pepstatin A and E-64 (LPE), nor the anti-VEGF antibody, blocked VEGFR2 suppression in response to HGF, stabilizing the Endo H-sensitive ER pool of VEGFR2 protein (Figs. 4E and S4A).

Lysine 48 (K48)-linked ubiquitination of protein substrates typically precedes their proteasomal destruction (Bonifacino and Weissman, 1998). We therefore examined whether VEGFR2 is thus ubiquitinated. IP of VEGFR2 under denaturing conditions (to strip away non-covalently attached proteins), followed by a K48-ubiquitin-specific IB, revealed constitutive baseline K48 ubiquitination of VEGFR2 in H441 cells (Figs. 4F and S4B). The K48-ubiquitinated fraction of VEGFR2 increased with MG132, and rose further in response to HGF alone or HGF plus MG132; in contrast, exogenous VEGF only minimally impacted this modification (Fig. 4F). In agreement with other findings (Ewan et al., 2006), the shift in gel migration of VEGFR2 suggested conjugation of 1–2 ubiquitin moieties. Importantly, HGF treatment increased K48 ubiquitination of VEGFR2 while decreasing total VEGFR2, whereas MET knockdown blocked K48 conjugation while increasing total VEGFR2 (Fig. 4G). Deubiquitinase treatment of VEGFR2 IPs from H441 and PC3 cells diminished the amount of K48 ubiquitin detected (Fig. S4B,C), further confirming HGF-induced K48 ubiquitination of VEGFR2. Previous work identifies the E3 ubiquitin ligase Cbl as responsible for VEGFR2 ubiquitination in endothelial cells in response to extracellular VEGF (Duval et al., 2003; Ewan et al., 2006). However, siRNA knockdown of Cbl, or its relative Cbl-b, which significantly depleted each target protein, did not affect the baseline level of VEGFR2 or its up-regulation by MET knockdown in H441 cells (Fig. S4D,E). Thus, unlike extracellular VEGF, MET promotes Cbl- and Cbl-b-independent K48 ubiquitination of VEGFR2. Whether MET-driven phosphorylation of VEGFR2 is a pre-requisite for its K48 ubiquitination and degradation remains to be investigated.

3.5. MET Depletes VEGFR2 via IRE1α-supported ERAD

Based on the above findings, we reasoned that the process known as ER-associated degradation (ERAD) (Vembar and Brodsky, 2008) might be involved in the depletion of VEGFR2 in response to MET activity. Although ERAD constitutively eliminates misfolded or aggregated polypeptides from the ER, it has been implicated also in modulating basal cellular levels of certain proteins (Hirsch et al., 2009). The E3 ligases HRD1 and gp78 as well as the chaperone p97/VCP play important roles in ERAD-mediated disposal of soluble and transmembrane protein substrates (Bernasconi et al., 2010; Vembar and Brodsky, 2008; Hirsch et al., 2009). Strikingly, siRNA knockdown of HRD1, gp78, or VCP substantially reversed VEGFR2 suppression by HGF in both PC3 and H441 cells (Figs. 5A and S5A–E). Furthermore, knockdown of HRD1 and gp78, but not Cbl, decreased the ratio of K48-ubiquitinated over total VEGFR2 protein in PC3 cells—both before and after treatment with HGF—reversing HGF-induced VEGFR2 suppression (Figs. 5B and S5F). Thus, E3 ligases that support ERAD are required for K48 ubiquitination and proteasomal degradation of VEGFR2 in response to MET signaling.

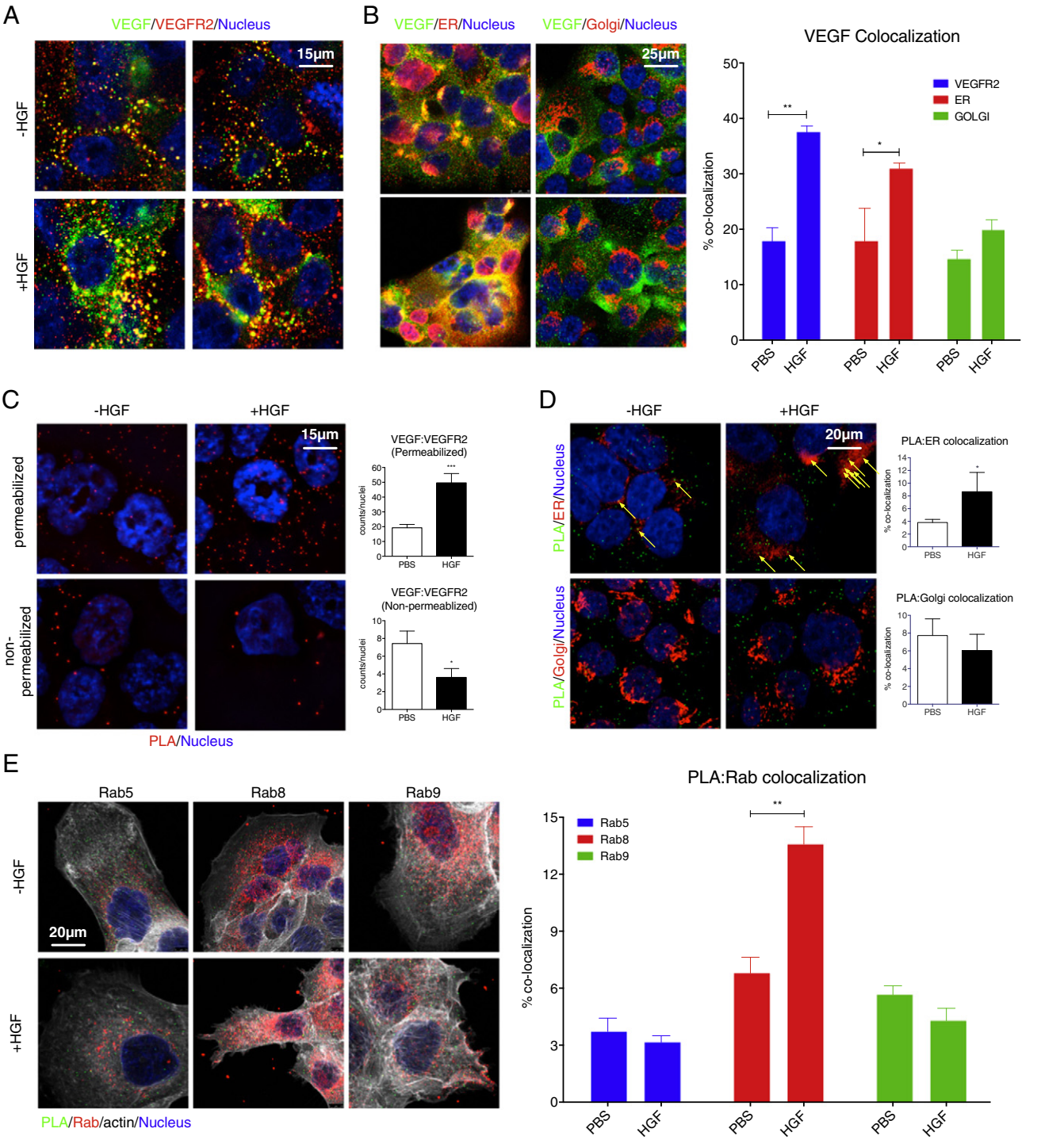

Fig. 3. HGF induces intracellular association of VEGF and VEGFR2. (A and B) H441 cells were treated with vehicle or HGF (100 ng/ml) for 24 h, fixed and stained for immunofluorescence with anti-VEGF (green), anti-VEGFR2 (red) and DAPI (Nucleus, blue) (A), or anti-VEGF (green), anti-ER or Golgi marker (red), and DAPI (blue) (B). VEGF colocalization with VEGFR2, ER or Golgi was quantitated (B, right panel). Nuclear stain is DAPI (blue). Error bars indicate S.E.M., n = 3; $^{**}p < 0.01$; $^{*}p < 0.05$ for indicated comparisons. (C) Cells were treated as above, and analyzed by proximity ligation assay (PLA) with quantification (right) with or without permeabilization. Red dots denote regions of signal amplification for VEGF:VEGFR2 proximity ligation. Nuclear stain is DAPI (blue). Error bars indicate S.E.M., n = 4; $^{***}p < 0.005$; $^{*}p < 0.05$ for indicated comparisons. (D) Cells were treated as in (C), permeabilized, and PLA was counterstained with either the ER marker (top) or Golgi marker (bottom). Green dots denote VEGF:VEGFR2 association. ER or Golgi stain is red and nuclear stain is blue. Colocalization between PLA signal and ER or Golgi staining is quantified (right). Error bars indicate S.E.M., n = 3; $^{*}p < 0.05$, arrows denote colocalized signal. (E) Cells were treated as above and PLA (green) was counterstained with indicated anti-Rab antibody (red), with nuclear stain (blue). Colocalization between PLA and Rab signals was quantified as in (D). Error bars indicate S.E.M., n = 3; $^{**}p < 0.01$ for indicated comparison.

The ERAD machinery is maintained and modulated by the unfolded protein response (UPR) (Brodsky, 2012; Hetz and Glimcher, 2009; Walter and Ron, 2011). Inositol-requiring enzyme 1α (IRE1α)—a key component of the UPR—activates the transcription factor X box protein-1 spliced (XBP-1s) to turn on multiple ERAD-linked genes in response to ER stress. Remarkably, HGF treatment of PC3 cells, which are more responsive to HGF than H441 cells, induced a time-dependent, biphasic increase in XBP-1s protein, and this was further enhanced by knockdown of

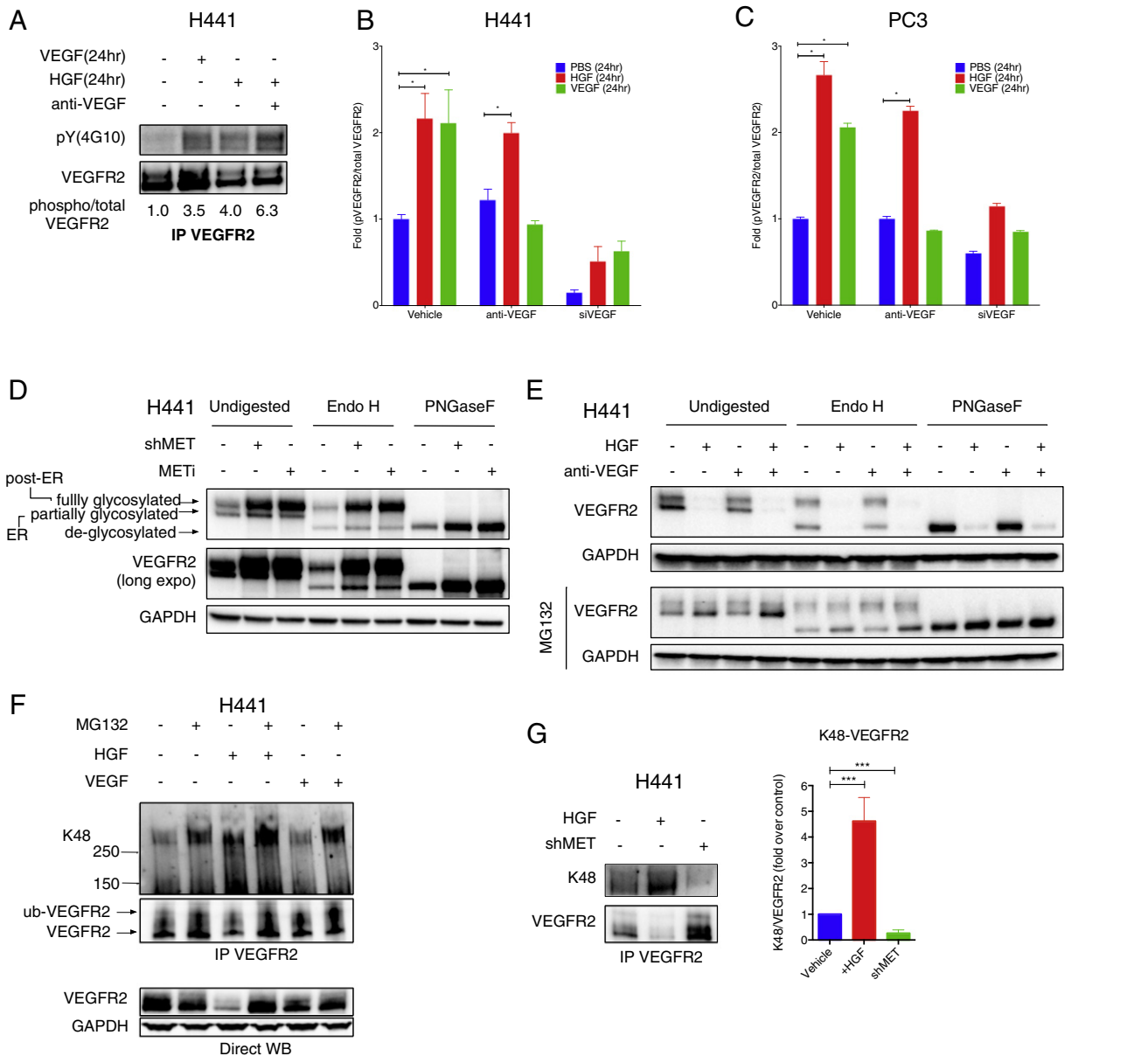

Fig. 4. HGF induces post-translational modification of VEGFR2. (A) Effect of exogenous VEGF or HGF on VEGFR2 phosphorylation. H441 cells were cultured with Na_3VO_4 (100 μM) and treated with HGF or VEGF (100 ng/ml) in the presence or absence of anti-VEGF antibody (10 μg/ml). Cell lysates were then subjected to VEGFR2 IP and analyzed by immunoblot phospho-VEGFR2 (top) or total VEGFR2 (bottom). (B) H441 cells were treated as in A and phospho-VEGFR2 or total VEGFR2 levels were measured by ELISA. VEGF knockdown (siVEGF) was tested for comparison. Error bars indicate S.E.M., n = 3; *p < 0.05 for indicated comparison. (C) Same as (B) for PC3 cells. (D) Effect of Endo H or PNGaseF digestion on migration of VEGFR2. H441 cells were treated with or without shMET or METi (GDC-0712, 1 μM) for 24 h. Cell lysates were then incubated with buffer (undigested), Endo H, or PNGaseF and VEGFR2 and MET were analyzed by IB. (E) (Left panel) Effect of proteasome inhibitors on HGF modulation of VEGFR2. H441 cells were treated with HGF (100 ng/ml) with or without anti-VEGF (10 μg/ml) for 24 h in absence or presence of MG132 (10 μM) and VEGFR2 levels were analyzed by IB. (Middle and right panels) same samples as shown in left panel but treated with either Endo H or PNGaseF. (F) Effect of HGF or VEGF on K48-linked ubiquitination of VEGFR2. H441 cells were treated with 100 ng/ml HGF or VEGF in the absence or presence of MG132 (10 μM). Cell lysates were subjected to VEGFR2 IP under denaturing conditions and immunoblotted with K48-ubiquitin antibody (top) or analyzed by direct VEGFR2 immunoblot (bottom). (G) H441 cells were treated with HGF (100 ng/ml) or subjected to MET knockdown (shMET) and K48-ubiquitinated or total VEGFR2 was detected as in E. Densitometric analysis of several experiments is shown on the right. Error bars indicate S.E.M., n = 5; ***p < 0.005 for indicated comparison.

HRD1 and gp78 in conjunction with stabilization of VEGFR2 (Fig. 5C). HGF also upregulated IRE1α phosphorylation, along with other UPR activation markers, namely ATF6 and BIP, but not PERK or its target C/EBP-homologous protein (CHOP) (Fig. S5G). SMI blockade of either IRE1α kinase (Wang et al., 2012) or RNase (Cross et al., 2012; Lu et al., 2014), but not PERK inhibition (Axten et al., 2012), attenuated XBP-1s upregulation by HGF (Figs. 5D, S5H,I), confirming a requirement for IRE1α activity. Thus, MET activity suppresses VEGFR2 via the ERAD machinery, which is supported by IRE1α activation.

Since both the VEGF and VEGFR2 polypeptides fold in the ER, we reasoned that their association within this organelle might drive the observed activation of IRE1α. Supporting this, SMI blockade of the PI3K/AKT pathway, which inhibited HGF-induced VEGF biosynthesis (Fig. 2D and G), substantially attenuated HGF-dependent upregulation of XBP-1s, as well as VEGFR2 depletion (Fig. 5E). Furthermore, siRNA knockdown of VEGF and VEGFR2 also attenuated generation of XBP-1s in response to HGF (Fig. 5F). In contrast, prolonged exposure to exogenous VEGF did not lead to generation of XBP-1s or degradation of VEGFR2, as compared to HGF exposure (Fig. S5J). Together, these results suggest that the HGF/MET-induced intracellular interaction between VEGF and VEGFR2 triggers IRE1α-supported, ERAD-mediated VEGFR2 disposal.

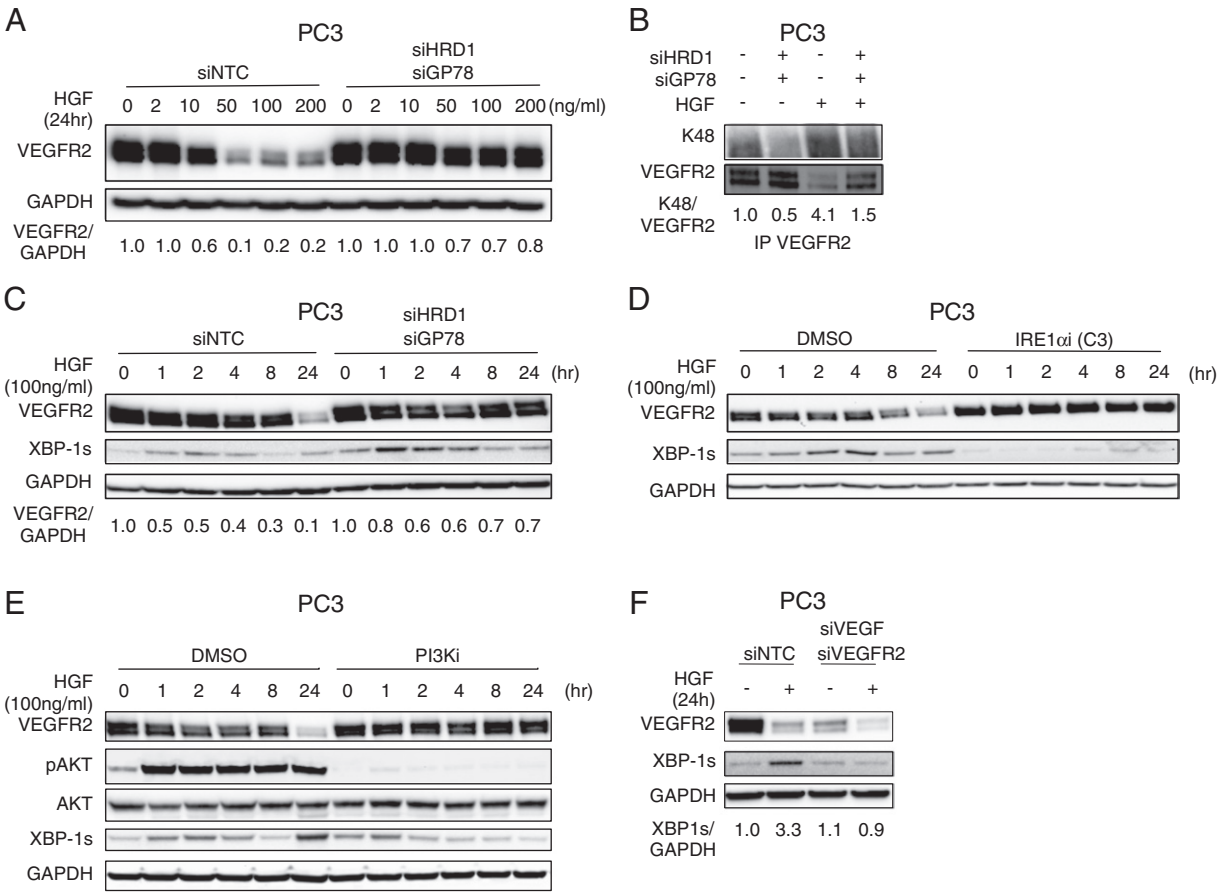

Fig. 5. HGF induces VEGFR2 depletion via IRE1α/XBP-1s and ERAD. (A) Effect of HRD1 and gp78 knockdown on HGF modulation of VEGFR2. PC3 cells were transfected with control siRNA or siRNAs targeting HRD1 and gp78 for 48 h, treated with HGF at the indicated concentration for 24 h, and analyzed by immunoblot. (B) PC3 cells were subjected to siRNA knockdown as in A, treated with vehicle or HGF (100 ng/ml) for 24 h, and K48-linked VEGFR2 was analyzed by immunoblot. (C) PC3 cells were treated as in (B) for the indicated time. Total VEGFR2 and spliced XBP-1 (XBP-1s) levels were then analyzed by immunoblot. Densitometric analysis of VEGFR2 normalized to GAPDH is shown below. (D) PC3 cells were treated with HGF for the indicated time in the presence of either vehicle (DMSO) or 10 μM IRE1α kinase inhibitors (Compound 3); VEGFR2 and XBP-1s levels were analyzed by immunoblot. (E) Cells were treated as in (D) in presence of vehicle or 10 μM PI3K inhibitor (GDC-0941). VEGFR2, phospho-AKT/total AKT, and XBP-1s were then analyzed by immunoblot. (F) PC3 cells were transfected with scrambled siRNA (siNTC), or siRNA against VEGF (siVEGF) and VEGFR2 (siVEGFR2) for 48 h. Cells were then treated with vehicle or HGF (100 ng/ml). VEGFR2 and XBP-1s levels were then analyzed by immunoblot. Densitometric analysis of XBP-1s normalized to GAPDH is shown below.

3.6. VEGFR2 Drives Compensatory Proliferation, Circumvented by Blockade of the MET and VEGFR2 Pathways

To interrogate the potential biological outcome of VEGFR2 modulation by MET, we measured possible changes in cell growth. H441 cells exhibited an increase of ~40% in number over a 3-day culture in serum-free medium, and MET knockdown or inhibition attenuated this growth by 2–3 fold (Fig. 6A). siRNA knockdown of VEGF or SMI blockade of PI3K also attenuated proliferation, and each treatment further increased the growth inhibition afforded by MET disruption. In contrast, anti-VEGF antibody did not affect cell growth either at baseline or upon MET perturbation. These results suggested that PI3K-dependent signaling and intracrine VEGF activity account for part of the observed MET-driven proliferation. Consistent with this, knockdown of either MET or VEGF downregulated intracellular VEGF, while combined knockdown of both targets led to a further drop in VEGF levels (Fig. 6B). MET knockdown increased not only total VEGFR2 protein, but also phosphorylated VEGFR2 (Fig. 6C), suggesting elevated VEGFR2 activity. Given that MET knockdown downregulated both the intracellular and secreted VEGF pools, this increase might reflect ligand-independent VEGFR2 autophosphorylation. Importantly, combined knockdown of MET and VEGFR2 led to stronger growth inhibition than did MET knockdown alone (Fig. 6D). Thus, increased VEGFR2 activity drives significant compensatory growth in the context of MET perturbation.

In keeping with previous data (Chaudhuri et al., 2011), MET disruption decreased phosphorylation of MET and its downstream mediators Gab1, PLC, and AKT; however, phosphorylation of MEK and ERK increased (Fig. 6E). SMI blockade of VEGFR2 attenuated the increase in MEK and ERK phosphorylation, whereas PI3K blockade did not (Fig. 6F). MET inhibition also augmented ERK phosphorylation in H2347 and LKPH4 cells, and this was reversed by VEGFR2 knockdown or inhibition (Fig. S6A,B). Given that PI3K inhibition prevents VEGF induction, these data raise the possibility that activation of the MEK–ERK pathway in the context of MET disruption may be mediated by VEGF-independent autophosphorylation of VEGFR2. Nevertheless, MET knockdown, which markedly upregulated VEGFR2, also increased cellular responsiveness to exogenous VEGF, as evident by significantly higher VEGFR2 phosphorylation as well as proliferation in response to VEGF addition (Fig. 6G and H). Moreover, whereas exogenous VEGF induced only a modest increase in baseline H441 cell growth, it increased proliferation more significantly in the context of MET knockdown (Figs. 6H and S6C). These results suggest that VEGFR2 upregulation upon MET disruption promotes compensatory MEK/ERK phosphorylation and proliferation via autophosphorylation of VEGFR2, as well as increases responsiveness to extracellular VEGF. Supporting this, SMI blockade of PI3K did not significantly alter VEGF-induced growth of MET-depleted cells, whereas MEK inhibition completely blocked proliferation (Fig. 6H). Furthermore, concurrent SMI blockade of MET and MEK had a stronger growth-inhibitory effect than did either SMI alone

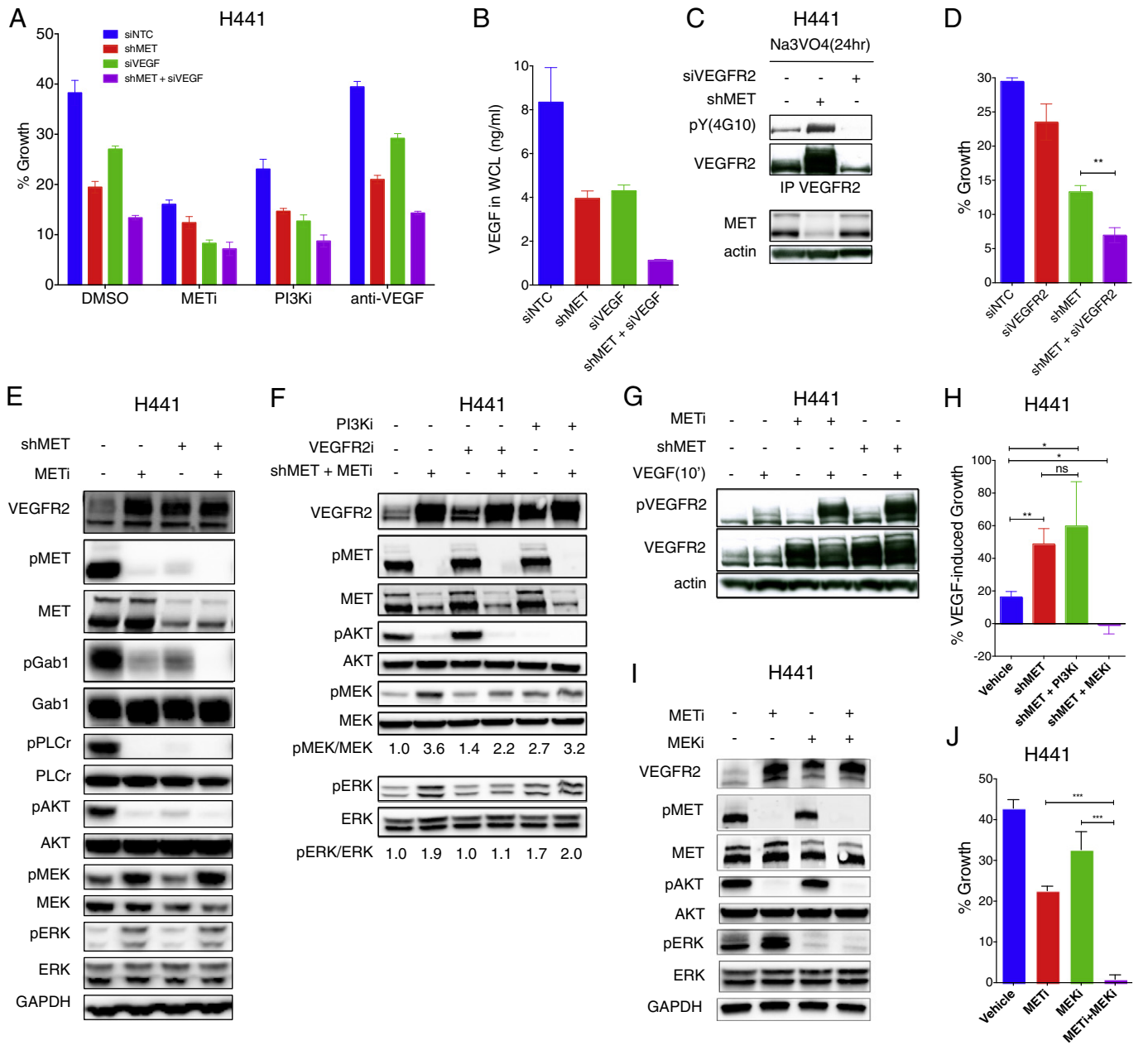

Fig. 6. VEGFR2 upregulation upon MET disruption facilitates compensatory cell growth. (A) Effect of MET or VEGF knockdown on cell growth. H441 cells were subjected to knockdown of MET (shMET) or VEGF (siVEGF) for 48 h and analyzed at 72 h for growth under the indicated treatment. (B) VEGF concentration in whole cell lysates from (A). (C) H441 cells were subjected to knockdown of MET (shMET) or VEGFR2 (siVEGFR2) for 48 h and incubated with activated sodium ortho-vanadate (Na_3VO_4) for 24 h. Total and phospho-VEGFR2 were then analyzed by IP and immunoblot. (D) H441 cells were subjected to knockdown of MET (shMET) or VEGFR2 (siVEGFR2) or both and analyzed for growth as in A. Error bars indicate S.E.M., n = 3; $^{**}p < 0.01$ for indicated comparison. (E) Effect of MET disruption on VEGFR2 levels and on downstream signaling. H441 cells were treated with or without shMET or METi (GDC-0712, 1 μM) for 24 h and analyzed for indicated markers by immunoblot. (F) Effect of VEGFR2 kinase inhibitor (su4312, 4 μM) and PI3K inhibitor (GDC-0941, 1 μM) on phosphorylation of downstream markers upon MET knockdown or inhibition in H441 cells. Densitometric analyses were normalized to the no MET inhibition. (G) Effect of MET shRNA knockdown (shMET) or inhibition (METi, 1 μM) on VEGFR2 and pVEGFR2 levels in H441 cells with or without addition of exogenous VEGF (100 ng/ml) for 10 min. (H) H441 cells were treated with or without VEGF (100 ng/ml) for 5 days in the presence of vehicle or Dox (shMET). Cells were treated with PBS, PI3Ki (GDC-0941, 1 μM) or MEKi (cobimetinib, 1 μM). Growth % was then analyzed by Incucyte. Error bars indicate S.E.M., n = 4; $^{*}p < 0.05$; $^{**}p < 0.01$ for indicated comparison. (I) Effect of MET inhibitor (GDC-0712, 1 μM) and MEK inhibitor (cobimetinib, 1 μM) on phosphorylation of downstream markers in H441 cells. (J) H441 cells were subjected to SMI blockade of MET (GDC-0712, 1 μM) or MEK (cobimetinib, 1 μM) or both and analyzed for growth as in A. Error bars indicate S.E.M., n = 5; $^{***}p < 0.005$ for indicated comparison.

(Fig. 6I and J). Moreover, VEGF knockdown on top of MET disruption led to an increase in VEGFR2 protein and enhanced VEGFR2 phosphorylation in response to exogenous VEGF (Fig. S6D,E). Thus, VEGFR2 upregulation restricts the growth inhibition afforded by MET disruption, particularly in the presence of extracellular VEGF.

In vivo, extracellular VEGF is often abundantly present in tumors. We reasoned that this might limit the effectiveness of MET-disruptive therapy, by driving compensatory growth via the upregulated VEGFR2. To investigate this, we xenografted H441 cells subcutaneously into mice and allowed them to establish tumors of ~200 mm^3. In vehicle-treated mice, tumors grew to ~1400 mm^3 over a period of ~50 days (Fig. 7A). Dox-induced MET knockdown or treatment with a neutralizing anti-VEGF antibody (B20.4.1.1) each attenuated growth of the pre-established tumors by ~50% (mean tumor volume 1360 mm^3, control, 840 mm^3, Dox, 760 mm^3, anti-VEGF). Remarkably however, a combination of both interventions led to a complete inhibition of tumor growth. In contrast, Dox treatment of H441 xenografts harboring a GFP shRNA as a control did not alter tumor growth or the inhibition thereof by anti-VEGF antibody

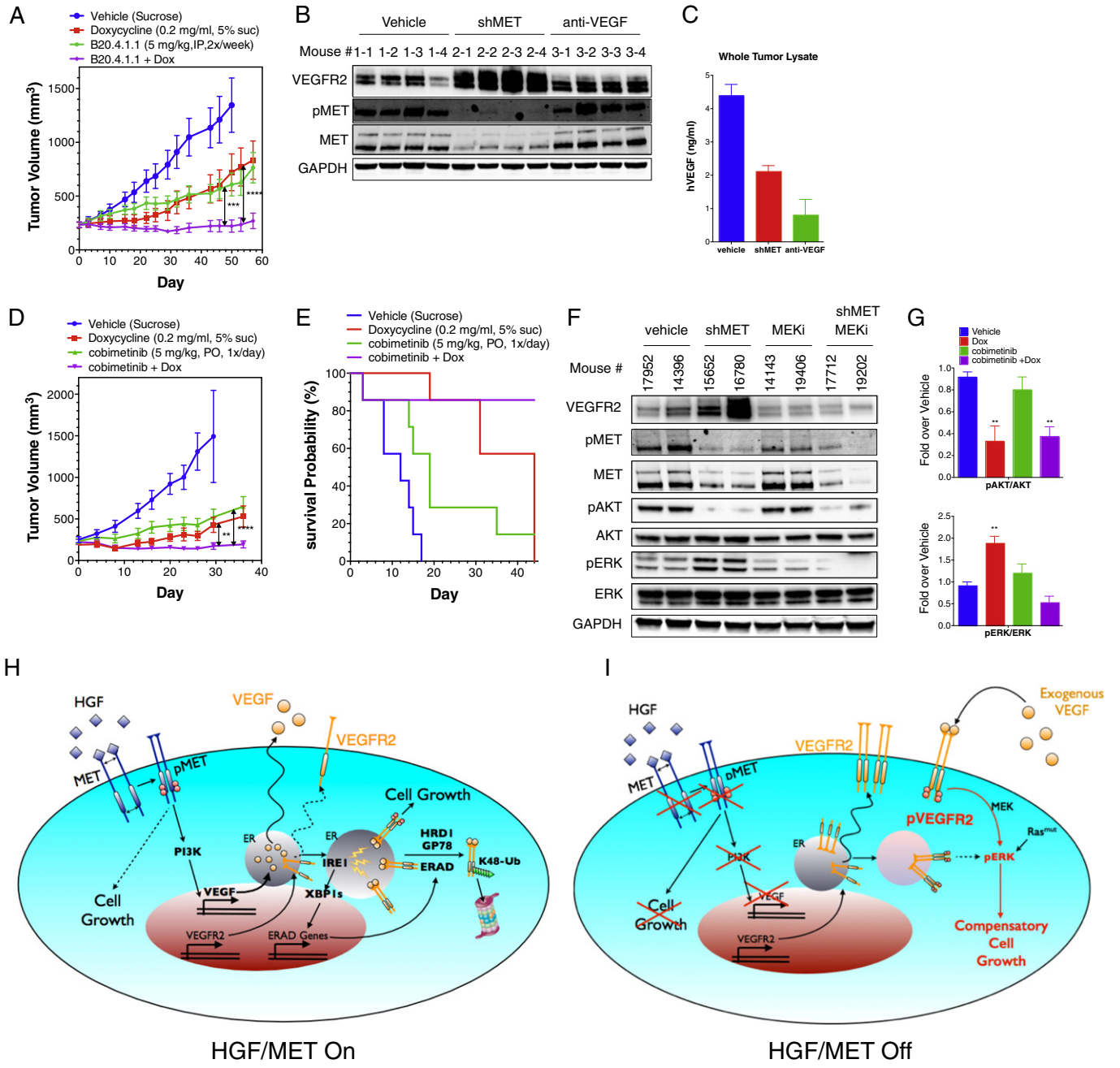

Fig. 7. Combined inhibition of MET and VEGF blocks tumor growth. (A) Effect of MET knockdown, VEGF neutralization, or both treatments on in vivo tumor growth. H441 shMET cells were injected subcutaneously into mice and tumors were allowed to grow and reach a volume of ~200 mm^2. Mice were then randomized into 4 groups and treated i.p. with vehicle (sucrose), Dox (0.2 mg/ml), anti-VEGF neutralizing antibody (B20-4.1.1, dosed at 5 mg/kg, twice per week), or Dox plus anti-VEGF antibody and tumor volume was monitored for the indicated time period. Error bars indicate S.E.M., ***$p < 0.005$; ****$p < 0.001$ for indicated comparison. (B and C) End-of-study tumor samples (n = 4 per group) were analyzed by immunoblot for VEGFR2, phospho-MET and MET protein (B) or by VEGF ELISA (C). (D) Effect of MET knockdown, MEK inhibition, or both treatments on tumor growth. H441 tumors were established as in A. Mice were randomized into 4 groups and treated with vehicle (sucrose), Dox (0.2 mg/ml), MEK SMI (cobimetinib, dosed p.o. at 5 mg/kg once per day), or Dox plus MEK SMI and tumor volume was monitored for the indicated time period. Error bars indicate S.E.M., **$p < 0.01$; ****$p < 0.001$ for indicated comparison. (E) Survival probability was calculated based on 2 times the initial tumor size as the threshold predicting death. (F) End-of-study tumor samples were analyzed by immunoblot for VEGFR2, phospho-MET, MET, phospho-AKT, AKT, phospho-ERK and ERK protein. (G) Densitometric analysis of phospho-AKT/AKT or phospho-ERK/ERK for end-of-study tumor samples. Error bars indicate S.E.M., n = 5 per group; **$p < 0.01$ for indicated comparison. (H and I) Model depicting cellular events in the context of HGF–MET activation or its disruption. (H) HGF–MET signaling induces VEGF production via the PI3K pathway. Newly synthesized VEGF and VEGFR2 proteins are folded in the ER. Premature interaction between VEGF and VEGFR2 within the ER activates IRE1α, leading to XBP-1 splicing and upregulation of ERAD genes. The ERAD-associated E3 ligases, HRD1 and gp78, mediate K48-linked ubiquitination of VEGFR2, leading to its proteasomal degradation. HGF–MET signaling is the main epithelial growth driver in this context. (I) MET disruption prevents PI3K-mediated VEGF induction. VEGFR2 is no longer directed to ERAD-mediated destruction and its upregulation leads to autophosphorylation as well as enhanced sensitivity to exogenous VEGF. While MET disruption blocks MET-stimulated growth, enhanced VEGFR2 signaling now drives compensatory proliferation. In tumors expressing both MET and VEGFR2 in the epithelial compartment, this compensatory growth limits the efficacy of MET-disruptive therapy. However, combined inhibition of both the HGF–MET and VEGF–VEGFR2 pathways overcomes this limitation and prevents tumor growth.

(Fig. S7A). To probe the underlying events upon MET knockdown, we analyzed end-of-study tumor samples by IB for levels of VEGFR2 and MET or by ELISA for levels of epithelial-derived human (h) VEGF. Dox treatment of H441 tumors harboring MET shRNA induced a substantial MET knockdown, strongly inhibiting MET phosphorylation; MET perturbation was associated with marked upregulation of VEGFR2 protein (Fig. 7B), and decreased the available amount of hVEGF in tumors by approximately one half (Fig. 7C). In contrast, anti-VEGF treatment only slightly affected

VEGFR2 levels, but depleted most of the free tumor-associated hVEGF (Fig. 7B and C). Furthermore, in an independent study, combined MET perturbation and MEK inhibition also led to complete attenuation of tumor growth, whereas each monotherapy enabled only partial inhibition (Fig. 7D and E). IB analysis of end-of-study tumor samples revealed that MET disruption inhibited AKT phosphorylation while upregulating VEGFR2 and inducing ERK phosphorylation; on the other hand, MEK inhibition attenuated phosphorylation of ERK but not AKT, whereas combined perturbation of MET and MEK blocked both phosphorylation events (Fig. 7F and G). Consistent with the enhanced growth inhibition of H441 tumors, combined inhibition of MET and MEK also led to significantly greater inhibition of growth of LKPH4 and PC3 cells in 2D or 3D in vitro cultures, respectively (Fig. S7B–E). Together, these results suggest that VEGFR2 upregulation upon MET disruption facilitates compensatory tumor growth in response to residual VEGF in tumors. Importantly, concurrent inhibition of either MET and VEGF or MET and MEK circumvents this compensation and provides significantly more profound inhibition of tumor growth.

4. Discussion

RTK pathways often regulate one another, and crosstalk between specific RTKs facilitates not only malignant tumor growth, but also resistance to cancer therapy. While epithelial signaling by HGF-MET primarily controls cell migration and invasiveness, there is evidence that MET also drives cell proliferation (Gherardi et al., 2012). The role of VEGF and VEGFR2 in modulating tumor-vascular growth and function is well established, both in preclinical models and in cancer patients (Ellis and Hicklin, 2008). Additionally, in tumor epithelial cells, the VEGF–VEGFR2 pathway can cooperate with EGFR signaling to promote proliferation (Lichtenberger et al., 2010). In contrast, in glioblastoma multiforme, VEGFR2 counteracts MET signaling and tumor invasiveness by facilitating MET dephosphorylation (Lu et al., 2012). Much less is known, however, about potential interactions between the VEGF–VEGFR2 and HGF–MET pathways in epithelial cancer cells and the resulting impact on tumor growth. Given this paucity of data, and the strong implication of both the VEGF–VEGFR2 and HGF–MET cascades as therapeutic targets in NSCLC, we were interested in finding out whether these two RTK pathways might interact in epithelial cancer cells in a biologically meaningful manner. Our studies reveal that MET signaling suppresses VEGFR2 activity in cell lines that express both RTKs. HGF–MET signaling via PI3K exerts negative control over VEGFR2 through a cell-autonomous mechanism that involves intracrine VEGF action and consequent ERAD-mediated depletion of VEGFR2 (Fig. 7H). In contrast, MET disruption upregulates VEGFR2, which facilitates compensatory tumor-cell proliferation (Fig. 7I). This unintended outcome limits the efficacy of MET-disrupting monotherapy; further proliferation may also be driven by aberrant mutational activation of the RAS–MEK pathway. However, compensatory growth can be circumvented by combined disruption of the MET and VEGFR2 or MET and MEK pathways to achieve complete suppression of tumor growth. Given the role of PI3K in VEGF upregulation, it is possible that a similar combinatorial strategy would enhance anti-tumor activity of PI3K inhibitors, as is the case for MET inhibitors.

Consistent with previous data (Bonnesen et al., 2009; Carrillo de Santa Pau et al., 2009), we observed endothelial VEGFR2 expression in most of the 31 NSCLC primary tumors analyzed. We also detected epithelial mRNA and protein expression of VEGFR2 in a small yet significant subset of lung adenocarcinomas. Further microarray analysis of patient-derived tumor samples showed elevated MET and VEGFR2 co-expression in additional lung cancer subsets. Given the substantial prevalence, morbidity and mortality of lung-associated malignancy, this fraction may represent a considerable number of patients. As MET-disruptive therapies progress through clinical studies, it is important to define how HGF–MET signaling interacts with other RTK pathways, e.g., VEGF–VEGFR2.

Our findings uncover an unprecedented mechanism of cross-regulation between two RTKs (Fig. 7H and I). Taken together, the data demonstrates that MET suppression of VEGFR2 requires PI3K-mediated biosynthesis of VEGF and intracrine VEGF activity. Several lines of evidence support this conclusion. First, VEGFR2 depletion required VEGF and could be induced by transfected or hypoxia-induced VEGF; however, it was independent of, and not stimulated by, extracellular VEGF. Second, inhibition of clathrin-mediated endocytosis with dynasore did not perturb MET modulation of VEGFR2. Third, HGF–MET signaling induced PI3K-dependent VEGF production and intracellular interaction between VEGF and VEGFR2 in conjunction with the ER. Association with vesicular structures marked by Rab8 also occurred, suggesting that some VEGF–VEGFR2 complexes may escape the ER toward the Golgi compartment. Fourth, MET disruption stabilized the Endo H-sensitive form of VEGFR2, which represents the partially glycosylated ER pool of the protein. Fifth, HGF addition, but not exogenous VEGF, promoted K48 ubiquitination of VEGFR2 and its proteasomal degradation. These data demonstrate an intracellular interaction of VEGF and VEGFR2, which may trigger the depletion of VEGFR2.

Extracellular VEGF binding induces internalization of VEGFR2 (Ewan et al., 2006), which appears to be important for efficient signaling (Chen et al., 2010; Sawamiphak et al., 2010). Moreover, exogenous VEGF induces ubiquitination of VEGFR2 via the E3 ligase Cbl, leading to proteasomal degradation of VEGFR2 (Duval et al., 2003). This destruction mechanism is unusual, given that most plasma membrane-bound RTKs undergo lysosomal rather than proteasomal degradation (Bonifacino and Weissman, 1998). Our data demonstrates that in contrast to extracellular VEGF, HGF–MET signaling induces K48 ubiquitination and depletion of VEGFR2 independently of Cbl or Cbl-b yet depending on the ERAD-associated E3 ligases HRD1 and gp78 and the chaperone p97 (VCP) (Bernasconi et al., 2010; Hirsch et al., 2009). HGF–MET activated IRE1α and its downstream transcriptional effector, XBP-1s—a UPR pathway crucial for ERAD maintenance—and this event was blocked by knockdown of VEGF and VEGFR2. Together, these results raise the intriguing hypothesis that interaction of newly synthesized VEGF and VEGFR2 proteins within the ER triggers activation of IRE1α and XBP-1s, thereby facilitating ERAD-mediated K48 ubiquitination and proteasomal disposal of VEGFR2. Supporting this, SMI blockade of IRE1α or XBP-1s prevented VEGFR2 suppression in response to HGF–MET signaling. Whether intracellular VEGF–VEGFR2 interaction requires VEGFR2 dimerization, and how this interaction drives IRE1α activation and ERAD remains to be investigated. One idea is that the massive upregulation of VEGF biosynthesis by HGF–MET signaling overwhelms ER folding capacity, thereby causing a premature, aberrant interaction between VEGF and VEGFR2. This may disrupt further maturation, leading to accumulation of misfolded VEGFR2 protein and its disposal via ERAD. Conceivably, VEGF degradation also could occur under such circumstances, but sufficient VEGF may escape these events to achieve secretion. It is notable in this context that the level of VEGF expressed by epithelial cancer cells is much higher than that produced by endothelial cells; moreover, although MET knockdown increased VEGFR2 phosphorylation in HUVEC, it did not significantly alter total VEGFR2 levels (data not shown). Thus, the low amount of VEGF expressed by HUVEC may be insufficient to suppress VEGFR2 at baseline, which would preclude endothelial VEGFR2 upregulation upon MET knockdown. Regardless, our data in epithelial cells uniquely identify a cell-autonomous mechanism that mediates cross-regulation not only between two distinct RTKs but also concerning a growth factor and its cognate receptor. Intracrine VEGF signaling was first proposed on the basis of evidence that wildtype, but not VEGF-null, endothelial cells exhibit VEGFR2 phosphorylation in the absence of exogenous VEGF; VEGFR2 phosphorylation was suppressed by VEGFR2 SMI, but not by anti-VEGF antibody, and was found to be crucial for vascular homeostasis (Lee et al., 2007). Further evidence supporting intracrine VEGF activity suggested that intracellular activation by VEGFR2 after the receptor is internalized and trafficked away from the plasma membrane is important for arterial

morphogenesis (Lanahan et al., 2010). Our data show that intracrine VEGF function can be regulated by MET signaling and plays a significant role in controlling VEGFR2 and associated growth of epithelial cancer cells.

In conclusion, our studies uncover a unique mechanism of cross-regulation between two RTKs that play crucial roles in tumor malignancy. Through this mechanism, MET suppresses VEGFR2 levels by promoting proteasomal degradation of VEGFR2. VEGF-blocking agents have established clinical utility in the treatment of NSCLC adenocarcinoma and of certain other epithelial cancers. Furthermore, several MET-disrupting agents, including antibodies and SMIs, are currently in NSCLC clinical trials. We found that MET disruption upregulates VEGFR2, thereby augmenting compensatory proliferation. Cell growth in the context of MET perturbation is driven both by VEGF-independent autophosphorylation of VEGFR2 and enhanced VEGFR2 signaling in response to extracellular VEGF, which activates of the MEK–ERK pathway (Fig. 7H and I). In vivo, MET perturbation in tumor epithelial cells is associated with a marked VEGFR2 upregulation; residual VEGF protein is detected in tumors and appears to drive further growth. Disruption of either MET, or VEGF, or MEK slowed tumor progression only partially; however, combined inhibition of MET and VEGF or MET and MEK completely blocked tumor growth. These findings have potentially important translational implications, particularly for tumors that display significant co-expression of MET and VEGFR2 in the malignant epithelial cell compartment. In such cases, the effectiveness of HGF–MET-disrupting monotherapy (or even its combination with other agents not targeting the VEGF–VEGFR2 pathway) may be offset by reactive growth driven by VEGFR2 upregulation and enhanced VEGF responsiveness. A promising strategy to overcome these limitations is to disrupt both RTK pathways together either at the ligand-receptor level or downstream.

Conflict of Interest

TC, JP, SM, HK, MM and AA are currently full-time employee of Genentech (a member of the Roche group). SM, MM and AA own stock shares of Roche, Inc. All authors declare no competing financial interests.

Acknowledgments

The authors thank Chris Servin and Jun Li for technical assistance, Jean-Michel Vernes, and Gloria Meng for ELISA consultation, Cecile Chalouni, Meredith Sagolla and László Kömüves for microscopy assistance, Linda Rangell and Murat Yaylaogle for IHC support, Klara Totpal for providing cancer cells to support in vivo studies, and Weilan Ye and members of the Ashkenazi lab for protocols, suggestions and discussions.

Appendix A. Supplementary Data

Supplementary data to this article can be found online at http://dx.doi.org/10.1016/j.ebiom.2015.03.021.

References

Axten, J.M., Medina, J.R., Feng, Y., Shu, A., Romeril, S.P., Grant, S.W., Li, W.H., Heerding, D.A., Minthorn, E., Mencken, T., Atkins, C., Liu, Q., Rabindran, S., Kumar, R., Hong, X., Goetz, A., Stanley, T., Taylor, J.D., Sigethy, S.D., Tomberlin, G.H., Hassell, A.M., Kahler, K.M., Shewchuk, L.M., Gampe, R.T., 2012. Discovery of 7-methyl-5-(1-{[3-(trifluoromethyl)phenyl]acetyl}-2,3-dihydro-1H-indol-5-yl)-7H-pyrrolo[2,3-d]pyrimidin-4-amine (GSK2606414), a potent and selective first-in-class inhibitor of protein kinase R (PKR)-like endoplasmic reticulum kinase (PERK). J. Med. Chem. 55, 7193–7207.

Bauer, T.W., Somcio, R.J., Fan, F., Liu, W., Johnson, M., Lesslie, D.P., Evans, D.B., Gallick, G.E., Ellis, L.M., 2006. Regulatory role of c-Met in insulin-like growth factor-I receptor-mediated migration and invasion of human pancreatic carcinoma cells. Mol. Cancer Ther. 5, 1676–1682.

Bernasconi, R., Galli, C., Calanca, V., Nakajima, T., Molinari, M., 2010. Stringent requirement for HRD1, SEL1L, and OS-9/XTP3-B for disposal of ERAD-LS substrates. J. Cell Biol. 188, 223–235.

Bonifacino, J.S., Weissman, A.M., 1998. Ubiquitin and the control of protein fate in the secretory and endocytic pathways. Annu. Rev. Cell Dev. Biol. 14, 19–57.

Bonnesen, B., Pappot, H., Holmstav, J., Skov, B.G., 2009. Vascular endothelial growth factor A and vascular endothelial growth factor receptor 2 expression in non-small cell lung cancer patients: relation to prognosis. Lung Cancer 66, 314–318.

Boon, E.M., Van Der Neut, R., Van De Wetering, M., Clevers, H., Pals, S.T., 2002. Wnt signaling regulates expression of the receptor tyrosine kinase met in colorectal cancer. Cancer Res. 62, 5126–5128.

Brodsky, J.L., 2012. Cleaning up: ER-associated degradation to the rescue. Cell 151, 1163–1167.

Carmeliet, P., Jain, R.K., 2011. Molecular mechanisms and clinical applications of angiogenesis. Nature 473, 298–307.

Carrillo De Santa Pau, E., Arias, F.C., Caso Pelaez, E., Munoz Molina, G.M., Sanchez Hernandez, I., Muguruza Trueba, I., Moreno Balsalobre, R., Sacristan Lopez, S., Gomez Pinillos, A., Del Val Toledo Lobo, M., 2009. Prognostic significance of the expression of vascular endothelial growth factors A, B, C, and D and their receptors R1, R2, and R3 in patients with nonsmall cell lung cancer. Cancer 115, 1701–1712.

Chaudhuri, A., Xie, M.H., Yang, B., Mahapatra, K., Liu, J., Marsters, S., Bodepudi, S., Ashkenazi, A., 2011. Distinct involvement of the Gab1 and Grb2 adaptor proteins in signal transduction by the related receptor tyrosine kinases RON and MET. J. Biol. Chem. 286, 32762–32774.

Chen, T.T., Luque, A., Lee, S., Anderson, S.M., Segura, T., Iruela-Arispe, M.L., 2010. Anchorage of VEGF to the extracellular matrix conveys differential signaling responses to endothelial cells. J. Cell Biol. 188, 595–609.

Chong, C.R., Janne, P.A., 2013. The quest to overcome resistance to EGFR-targeted therapies in cancer. Nat. Med. 19, 1389–1400.

Choura, M., Rebai, A., 2011. Receptor tyrosine kinases: from biology to pathology. J. Recept. Signal Transduct. Res. 31, 387–394.

Cross, B.C., Bond, P.J., Sadowski, P.G., Jha, B.K., Zak, J., Goodman, J.M., Silverman, R.H., Neubert, T.A., Baxendale, I.R., Ron, D., Harding, H.P., 2012. The molecular basis for selective inhibition of unconventional mRNA splicing by an IRE1-binding small molecule. Proc. Natl. Acad. Sci. U. S. A. 109, E869–E878.

Dong, G., Chen, Z., Li, Z.Y., Yeh, N.T., Bancroft, C.C., Van Waes, C., 2001. Hepatocyte growth factor/scatter factor-induced activation of MEK and PI3K signal pathways contributes to expression of proangiogenic cytokines interleukin-8 and vascular endothelial growth factor in head and neck squamous cell carcinoma. Cancer Res. 61, 5911–5918.

Duval, M., Bedard-Goulet, S., Delisle, C., Gratton, J.P., 2003. Vascular endothelial growth factor-dependent down-regulation of Flk-1/KDR involves Cbl-mediated ubiquitination. Consequences on nitric oxide production from endothelial cells. J. Biol. Chem. 278, 20091–20097.

Eder, J.P., Vande Woude, G.F., Boerner, S.A., Lorusso, P.M., 2009. Novel therapeutic inhibitors of the c-Met signaling pathway in cancer. Clin. Cancer Res. 15, 2207–2214.

Ellis, L.M., Hicklin, D.J., 2008. VEGF-targeted therapy: mechanisms of anti-tumour activity. Nat. Rev. Cancer 8, 579–591.

Engelman, J.A., Zejnullahu, K., Mitsudomi, T., Song, Y., Hyland, C., Park, J.O., Lindeman, N., Gale, C.M., Zhao, X., Christensen, J., Kosaka, T., Holmes, A.J., Rogers, A.M., Cappuzzo, F., Mok, T., Lee, C., Johnson, B.E., Cantley, L.C., Janne, P.A., 2007. MET amplification leads to gefitinib resistance in lung cancer by activating ERBB3 signaling. Science 316, 1039–1043.

Ewan, L.C., Jopling, H.M., Jia, H., Mittar, S., Bagherzadeh, A., Howell, G.J., Walker, J.H., Zachary, I.C., Ponnambalam, S., 2006. Intrinsic tyrosine kinase activity is required for vascular endothelial growth factor receptor 2 ubiquitination, sorting and degradation in endothelial cells. Traffic 7, 1270–1282.

Ferrara, N., Gerber, H.P., Lecouter, J., 2003. The biology of VEGF and its receptors. Nat. Med. 9, 669–676.

Forsythe, J.A., Jiang, B.H., Iyer, N.V., Agani, F., Leung, S.W., Koos, R.D., Semenza, G.L., 1996. Activation of vascular endothelial growth factor gene transcription by hypoxia-inducible factor 1. Mol. Cell. Biol. 16, 4604–4613.

Gautier, L., Cope, L., Bolstad, B.M., Irizarry, R.A., 2004. affy—analysis of Affymetrix GeneChip data at the probe level. Bioinformatics 20, 307–315.

Gavard, J., Gutkind, J.S., 2006. VEGF controls endothelial-cell permeability by promoting the beta-arrestin-dependent endocytosis of VE-cadherin. Nat. Cell Biol. 8, 1223–1234.

Gherardi, E., Birchmeier, W., Birchmeier, C., Vande Woude, G., 2012. Targeting MET in cancer: rationale and progress. Nat. Rev. Cancer 12, 89–103.

Glubb, D.M., Cerri, E., Giese, A., Zhang, W., Mirza, O., Thompson, E.E., Chen, P., Das, S., Jassem, J., Rzyman, W., Lingen, M.W., Salgia, R., Hirsch, F.R., Dziadziuszko, R., Ballmer-Hofer, K., Innocenti, F., 2011. Novel functional germline variants in the VEGF receptor 2 gene and their effect on gene expression and microvessel density in lung cancer. Clin. Cancer Res. 17, 5257–5267.

Goel, H.L., Mercurio, A.M., 2013. VEGF targets the tumour cell. Nat. Rev. Cancer 13, 871–882.

Gonzalvez, F., Lawrence, D., Yang, B., Yee, S., Pitti, R., Marsters, S., Pham, V.C., Stephan, J.P., Lill, J., Ashkenazi, A., 2012. TRAF2 Sets a threshold for extrinsic apoptosis by tagging caspase-8 with a ubiquitin shutoff timer. Mol. Cell 48, 888–899.

Gordon, J.A., 1991. Use of vanadate as protein-phosphotyrosine phosphatase inhibitor. Methods Enzymol. 201, 477–482.

He, Z., Opland, D.M., Way, K.J., Ueki, K., Bodyak, N., Kang, P.M., Izumo, S., Kulkarni, R.N., Wang, B., Liao, R., Kahn, C.R., King, G.L., 2006. Regulation of vascular endothelial growth factor expression and vascularization in the myocardium by insulin receptor and PI3K/Akt pathways in insulin resistance and ischemia. Arterioscler. Thromb. Vasc. Biol. 26, 787–793.

Hetz, C., Glimcher, L.H., 2009. Fine-tuning of the unfolded protein response: assembling the IRE1alpha interactome. Mol. Cell 35, 551–561.
Hirsch, C., Gauss, R., Horn, S.C., Neuber, O., Sommer, T., 2009. The ubiquitylation machinery of the endoplasmic reticulum. Nature 458, 453–460.
Jiang, B.H., Zheng, J.Z., Aoki, M., Vogt, P.K., 2000. Phosphatidylinositol 3-kinase signaling mediates angiogenesis and expression of vascular endothelial growth factor in endothelial cells. Proc. Natl. Acad. Sci. U. S. A. 97, 1749–1753.
Khoury, H., Naujokas, M.A., Zuo, D., Sangwan, V., Frigault, M.M., Petkiewicz, S., Dankort, D.L., Muller, W.J., Park, M., 2005. HGF converts ErbB2/Neu epithelial morphogenesis to cell invasion. Mol. Biol. Cell 16, 550–561.
Kowanetz, M., Ferrara, N., 2006. Vascular endothelial growth factor signaling pathways: therapeutic perspective. Clin. Cancer Res. 12, 5018–5022.
Lanahan, A.A., Hermans, K., Claes, F., Kerley-Hamilton, J.S., Zhuang, Z.W., Giordano, F.J., Carmeliet, P., Simons, M., 2010. VEGF receptor 2 endocytic trafficking regulates arterial morphogenesis. Dev. Cell 18, 713–724.
Lee, S., Chen, T.T., Barber, C.L., Jordan, M.C., Murdock, J., Desai, S., Ferrara, N., Nagy, A., Roos, K.P., Iruela-Arispe, M.L., 2007. Autocrine VEGF signaling is required for vascular homeostasis. Cell 130, 691–703.
Lichtenberger, B.M., Tan, P.K., Niederleithner, H., Ferrara, N., Petzelbauer, P., Sibilia, M., 2010. Autocrine VEGF signaling synergizes with EGFR in tumor cells to promote epithelial cancer development. Cell 140, 268–279.
Liederer, B.M., Berezhkovskiy, L.M., Dean, B.J., Dinkel, V., Peng, J., Merchant, M., Plise, E.G., Wong, H., Liu, X., 2011. Preclinical absorption, distribution, metabolism, excretion, and pharmacokinetic-pharmacodynamic modelling of N-(4-(3-((3S,4R)-1-ethyl-3-fluoropiperidine-4-ylamino)-1H-pyrazolo[3,4-b]pyridin-4-yloxy)-3-fluorophenyl)-2-(4-fluorophenyl)-3-oxo-2,3-dihydropyridazine-4-carboxamide, a novel MET kinase inhibitor. Xenobiotica 41, 327–339.
Liu, Y., Chattopadhyay, N., Qin, S., Szekeres, C., Vasylyeva, T., Mahoney, Z.X., Taglienti, M., Bates, C.M., Chapman, H.A., Miner, J.H., Kreidberg, J.A., 2009. Coordinate integrin and c-Met signaling regulate Wnt gene expression during epithelial morphogenesis. Development 136, 843–853.
Lu, K.V., Chang, J.P., Parachoniak, C.A., Pandika, M.M., Aghi, M.K., Meyronet, D., Isachenko, N., Fouse, S.D., Phillips, J.J., Cheresh, D.A., Park, M., Bergers, G., 2012. VEGF inhibits tumor cell invasion and mesenchymal transition through a MET/VEGFR2 complex. Cancer Cell 22, 21–35.
Lu, M., Lawrence, D.A., Marsters, S., Acosta-Alvear, D., Kimmig, P., Mendez, A.S., Paton, A.W., Paton, J.C., Walter, P., Ashkenazi, A., 2014. Cell death. Opposing unfolded-protein-response signals converge on death receptor 5 to control apoptosis. Science 345, 98–101.
Luque, A., Carpizo, D.R., Iruela-Arispe, M.L., 2003. ADAMTS1/METH1 inhibits endothelial cell proliferation by direct binding and sequestration of VEGF165. J. Biol. Chem. 278, 23656–23665.
Pai, R., Dunlap, D., Qing, J., Mohtashemi, I., Hotzel, K., French, D.M., 2008. Inhibition of fibroblast growth factor 19 reduces tumor growth by modulating beta-catenin signaling. Cancer Res. 68, 5086–5095.
Pegram, M., Hsu, S., Lewis, G., Pietras, R., Beryt, M., Sliwkowski, M., Coombs, D., Baly, D., Kabbinavar, F., Slamon, D., 1999. Inhibitory effects of combinations of HER-2/neu antibody and chemotherapeutic agents used for treatment of human breast cancers. Oncogene 18, 2241–2251.
Sadiq, A.A., Salgia, R., 2013. MET as a possible target for non-small-cell lung cancer. J. Clin. Oncol. 31, 1089–1096.
Sawamiphak, S., Seidel, S., Essmann, C.L., Wilkinson, G.A., Pitulescu, M.E., Acker, T., Acker-Palmer, A., 2010. Ephrin-B2 regulates VEGFR2 function in developmental and tumour angiogenesis. Nature 465, 487–491.
Smith, N.R., Baker, D., James, N.H., Ratcliffe, K., Jenkins, M., Ashton, S.E., Sproat, G., Swann, R., Gray, N., Ryan, A., Jurgensmeier, J.M., Womack, C., 2010. Vascular endothelial growth factor receptors VEGFR-2 and VEGFR-3 are localized primarily to the vasculature in human primary solid cancers. Clin. Cancer Res. 16, 3548–3561.
Soderberg, O., Gullberg, M., Jarvius, M., Ridderstrale, K., Leuchowius, K.J., Jarvius, J., Wester, K., Hydbring, P., Bahram, F., Larsson, L.G., Landegren, U., 2006. Direct observation of individual endogenous protein complexes in situ by proximity ligation. Nat. Methods 3, 995–1000.
Spigel, D.R., Ervin, T.J., Ramlau, R.A., Daniel, D.B., Goldschmidt Jr., J.H., Blumenschein Jr., G.R., Krzakowski, M.J., Robinet, G., Godbert, B., Barlesi, F., Govindan, R., Patel, T., Orlov, S.V., Wertheim, M.S., Yu, W., Zha, J., Yauch, R.L., Patel, P.H., Phan, S.C., Peterson, A.C., 2013. Randomized phase II trial of onartuzumab in combination with erlotinib in patients with advanced non-small-cell lung cancer. J. Clin. Oncol. 31, 4105–4114.
Takeuchi, K., Ito, F., 2011. Receptor tyrosine kinases and targeted cancer therapeutics. Biol. Pharm. Bull. 34, 1774–1780.
Turke, A.B., Zejnullahu, K., Wu, Y.L., Song, Y., Dias-Santagata, D., Lifshits, E., Toschi, L., Rogers, A., Mok, T., Sequist, L., Lindeman, N.I., Murphy, C., Akhavanfard, S., Yeap, B.Y., Xiao, Y., Capelletti, M., Iafrate, A.J., Lee, C., Christensen, J.G., Engelman, J.A., Janne, P.A., 2010. Preexistence and clonal selection of MET amplification in EGFR mutant NSCLC. Cancer Cell 17, 77–88.
Vembar, S.S., Brodsky, J.L., 2008. One step at a time: endoplasmic reticulum-associated degradation. Nat. Rev. Mol. Cell Biol. 9, 944–957.
Walter, P., Ron, D., 2011. The unfolded protein response: from stress pathway to homeostatic regulation. Science 334, 1081–1086.
Wang, L., Perera, B.G., Hari, S.B., Bhhatarai, B., Backes, B.J., Seeliger, M.A., Schurer, S.C., Oakes, S.A., Papa, F.R., Maly, D.J., 2012. Divergent allosteric control of the IRE1alpha endoribonuclease using kinase inhibitors. Nat. Chem. Biol. 8, 982–989.
Wilson, T.R., Fridlyand, J., Yan, Y., Penuel, E., Burton, L., Chan, E., Peng, J., Lin, E., Wang, Y., Sosman, J., Ribas, A., Li, J., Moffat, J., Sutherlin, D.P., Koeppen, H., Merchant, M., Neve, R., Settleman, J., 2012. Widespread potential for growth-factor-driven resistance to anticancer kinase inhibitors. Nature 487, 505–509.
Yamamoto, N., Mammadova, G., Song, R.X., Fukami, Y., Sato, K., 2006. Tyrosine phosphorylation of p145met mediated by EGFR and Src is required for serum-independent survival of human bladder carcinoma cells. J. Cell Sci. 119, 4623–4633.
Zhang, Y.W., Su, Y., Volpert, O.V., Vande Woude, G.F., 2003. Hepatocyte growth factor/scatter factor mediates angiogenesis through positive VEGF and negative thrombospondin 1 regulation. Proc. Natl. Acad. Sci. U. S. A. 100, 12718–12723.
Zhang, Z., Neiva, K.G., Lingen, M.W., Ellis, L.M., Nor, J.E., 2010. VEGF-dependent tumor angiogenesis requires inverse and reciprocal regulation of VEGFR1 and VEGFR2. Cell Death Differ. 17, 499–512.